3.13 Molten Salt Reactor Fuel and Coolant

O. Beneš and R. J. M. Konings
European Commission, Joint Research Centre, Institute for Transuranium Elements, Karlsruhe, Germany

© 2012 Elsevier Ltd. All rights reserved.

Abbreviations

AHTR	Advanced high-temperature reactor
ARE	Aircraft Reactor Experiment
CNRS	Centre National de la Recherche Scientifique
FLIBE	Eutectic mixture of LiF and BeF_2
MOSART	Molten Salt Actinide Recycler and Transmuter
MSBR	Molten salt breeder reactor
MS-FR	Molten salt cooled fast reactor
MSFR	Molten salt fast reactor
MSR	Molten salt reactor
MSRE	Molten Salt Reactor Experiment
ORNL	Oak Ridge National Laboratory
PWR	Pressurized water reactor
SFR	Sodium cooled fast reactor
VHTR	Very high-temperature reactor

3.13.1 Introduction

The molten salt reactor (MSR) is one of the six reactor concepts of the Generation IV initiative, which is an international collaboration to study the next generation nuclear power reactors. The fuel of the MSR is based on the dissolution of the fissile material (^{235}U, ^{233}U, or ^{239}Pu) in an inorganic liquid that is pumped at a low pressure through the reactor vessel and the primary circuit, and thus also serves as the primary coolant. The heat generated by the fission process is transferred in a heat exchanger to a secondary coolant, which is also generally a molten salt. This intermediate loop is introduced for safety reasons: to avoid direct contact between the steam and the fuel. A schematic drawing of the MSR is shown in **Figure 1** as taken from US DOE Roadmap.[1] The operating temperature of the MSR is between 800 and 1000 K, the lower limit being determined by the fusion temperature of the salt and the upper one by the corrosion rate of the structural material (see **Chapter 5.10, Material Performance in Molten Salts**). Typical inlet and outlet temperatures of some MSR concepts, which are briefly discussed in **Section 3.13.3**, are summarized in **Table 1**. It is worth mentioning that at least a 50 K safety margin must be kept in all concepts, and hence the melting temperature of the fuel salt must be at least 50 K lower than the designed inlet temperature of the reactor.

The fact that the fuel of the MSR is in the liquid state offers several advantages. The first among them is the safety of the reactor. As the fuel is in the liquid state and serves as primary coolant having low vapor pressures (boiling points >1400 °C), the total pressure of the primary circuit is kept very low ($p \sim 1$ bar) compared to, for example, current light water reactors. It thus avoids the major driving force, the high pressure, for radioactivity release during accidents. Another aspect that contributes to the safety of the MSR is that the reactor possesses a strong negative temperature coefficient, so the chain reaction automatically slows down when the temperature increases. This is induced by the thermal expansion of the primary coolant, which pushes the fuel out of the reactor core (the fuel density decreases). The third characteristic that increases the safety of the reactor is the possibility of draining the liquid fuel into emergency dump tanks in case of an accident. The emergency tanks are installed under the reactor and are designed in such way that the fuel remains in a subcritical state.

Another big advantage of the MSR is the possibility of performing a continuous fuel cleanup, which results in an increase of the fuel burnup. This chemical cleanup can be done either online or in batches. The goal of the fuel cleanup is to separate the fission products from the fuel and transfer them into the nuclear waste, while the cleaned fuel is sent back into the primary circuit. It is very important to make this separation because most of the fission products have a very high neutron capture

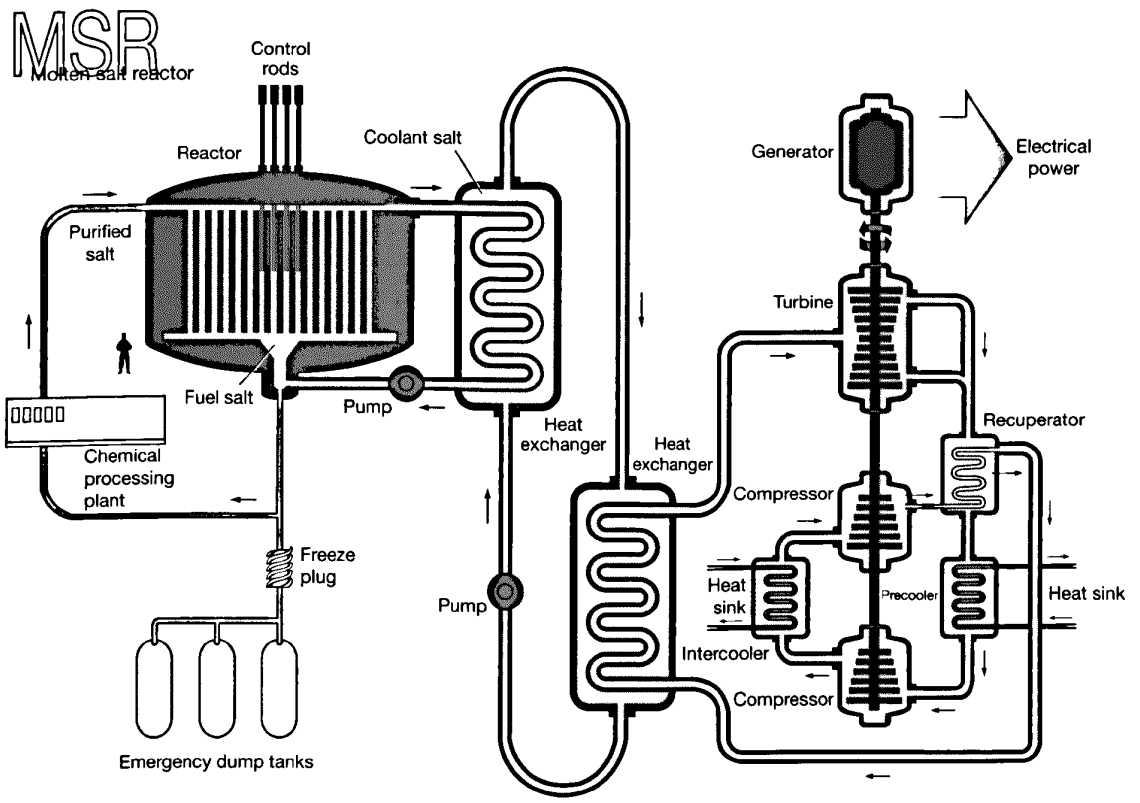

Figure 1 Schematic drawing of the molten salt reactor. Reproduced from US DOE Nuclear Energy Research Advisory Committee and the Generation IV International Forum, A Technology Roadmap for Generation IV Nuclear Energy Systems, http://www.ne.doe.gov/genIV/documents/gen_iv_roadmap.pdf © Generation IV International Forum.

Table 1 Typical fuel salt inlet and outlet temperatures of some MSR concepts

MSR concept	T_{inlet}	T_{outlet}	*References*
MSRE	908 K	936 K	2
MSBR	839 K	977 K	3
MSR FUJI	840 K	980 K	4
MSFR	903 K	923 K	5
MOSART	873 K	988 K	6

cross-section and thus slow down the chain reaction. Because of the online cleanup, a very low amount of fission products is present in the fuel during the reactor operation, and thus the heat generation from their radioactive decay is small and the risk of overheating in the event of loss of cooling is avoided. Moreover, it is also possible to profit from the neutron economy and design the MSR as a breeder reactor that produces more fuel than it consumes, for example, using a $^{232}Th/^{233}U$ cycle.

Furthermore, because of the liquid state of the MSR fuel, there is no radiation damage to the fuel (as discussed in **Section 3.13.7**). Therefore, issues such as swelling or crack formation that appear in the case of ceramic fabricated fuels are avoided.

3.13.2 Historical Background

The first proposal for a MSR dates back to the 1940s when Bettis and Briant proposed it for aircraft propulsion.[7] A substantial research program was started at the Oak Ridge National Laboratory (ORNL) in the United States to develop this idea, culminating in the Aircraft Reactor Experiment (ARE) that went critical for several days in 1954. However, no airplane with such propulsion has ever been constructed. For ARE, a mixture of $NaF–ZrF_4$ was used as carrier of the fissile UF_4 for the following reasons[8,9]:

- Wide range of solubility for thorium and uranium
- Thermodynamic stability up to high temperatures
- No radiolytic decomposition
- Low vapor pressure at the operating temperature of the reactor

- Compatibility with nickel-based alloys (Ni–Mo–Cr–Fe) that can be used as structural materials.

In the second half of the 1950s, the molten salt technology was transferred to the civilian nuclear program of the United States. At the time, many reactor concepts were being studied and the interest in breeder reactors was growing. It was recognized that the MSR would be ideal for thermal breeding of uranium from thorium,[7] and the Molten Salt Reactor Experiment (MSRE) was started at ORNL to demonstrate the operability of MSRs. Because of the breeding aspect, the neutron economy in the reactor was considered to be of key importance, and ^{7}LiF–BeF_2 (FLIBE), with 5% ZrF_4 as oxygen getter, was selected as fuel carrier because of the very low neutron capture cross-sections of ^{7}Li ($\sigma_{thermal} = 0.045$ barn) and Be ($\sigma_{thermal} = 0.0088$ barn). Natural lithium cannot be used as part of the nuclear fuel as it contains about 7.6% of ^{6}Li (the remaining 92.4% is ^{7}Li), which has a very high parasitic neutron capture cross-section ($\sigma_{thermal} = 940$ barn). Therefore, enrichment of ^{7}Li is required before it can be used as a fuel matrix. The MSRE was a graphite-moderated reactor of 8 MWth (megawatt thermal) and operated from 1965 to 1969. Two different fissile sources were used: initially, $^{235}UF_4$ was used with 33% enrichment and later, $^{233}UF_4$ was added to the carrier salt, making the MSRE the world's first reactor to be fueled with this fissile material.[10] FLIBE was used as coolant in the secondary circuit. The results of MSRE, which have been reported in great detail,[10] revealed that all the selected materials (fuel, structurals) behaved well and that the equipment behaved as predicted. In this respect, it was very successful.

After the MSRE, a design for a prototype molten salt breeder reactor (MSBR) was made by ORNL in the early 1970s.[3] The program was stopped in 1976 in favor of the liquid metal cooled fast reactor[7]: although the technology was considered promising, there were technological problems that had to be solved. The MSBR design was a 2250 MWth reactor, optimized to breed ^{233}U from ^{232}Th in a single fluid system. Online pyrochemical cleanup was planned to clean the fuel solvent from the neutron-absorbing fission products. Nevertheless, interruption of reactor operation was planned every 4 years to replace the graphite moderator, as experiments had revealed significant swelling of graphite due to radiation damage. Because of the (semi)continuous online clean up of the fuel, the addition of zirconium to the fuel was not necessary, and FLIBE could be used as carrier of the fertile (ThF_4) and fissile elements (UF_4). As secondary coolant, a NaF–$NaBF_4$ (8–92 mol%) mixture was foreseen, particularly because the tritium retention of this salt is much better than FLIBE.

In the 1990s, there was a renewed interest in molten salt technology, which originated from programs that were looking into the possibilities of transmutation of actinides. When addressing transmutation of minor actinides, the absence of complicated fuel and fuel pin fabrication and the compatibility with pyrochemical processing in the molten salt fuel cycle were recognized as important advantages, in comparison with conventional pellet fuel types. Also, the interest in the use of thorium as a nuclear fuel kept up the interest in MSRs. As a result, the MSR is now one of the six reactor concepts selected for the Generation IV initiative, which is looking at next generation nuclear reactors. Current MSR designs, however, move away from thermal graphite-moderated concepts, and favor nonmoderated concepts that have a fast(er) neutron spectrum. Fuel selection for the nonmoderated reactor concepts is more flexible, and elements other than ^{7}Li can be considered. One reason is that the neutron capture cross-section of the alkali halides and alkali-earth halides is generally lower in the 'fast' spectrum than in the thermal spectrum; also, the neutron economy is not as sensitive in the 'fast' spectrum as in the thermal one. Therefore compounds like NaF, KF, RbF, or CaF_2 can be considered as part of the fuel matrix. Moreover, there are some 'fast' MSR concepts, for example, the REBUS-3700 concept,[11] which are based on the chloride matrix (^{35}Cl: $\sigma_{fast} = 0.0011$ barn, whereas $\sigma_{thermal} = 43.63$ barn).

3.13.3 Fuel Concepts of MSR

The fuel in the MSR must fulfill several requirements with respect to its physicochemical properties (as will be discussed in **Section 3.13.4**). These requirements are very well met by the various systems containing alkali metal and alkali-earth fluorides; hence the fluoride systems are the most recognized candidates for MSR fuels.

In the previous section, the MSBR has been mentioned as a graphite-moderated reactor that is based on the ^{7}LiF–BeF_2–$^{232}ThF_4$–UF_4 system.[3] $^{232}ThF_4$ is a fertile material that is used to produce fissile $^{233}UF_4$ by a neutron capture and two consecutive β-decays of ^{233}Th and ^{233}Pa. This fuel composition based on the FLIBE matrix still remains an ideal candidate

when the MSR is designed as a thermal breeder reactor (moderated reactor). In this case, neutron economy is very critical and only isotopes with very low neutron capture cross-section in the thermal spectrum can be part of the fuel matrix. Thus, ^{7}LiF and BeF_2 are the prime compounds for consideration. One of the current MSR concepts that uses fuel technology similar to that of the MSBR is the MSR FUJI concept.[4] Originally proposed by Furukawa, it is a rather small graphite-moderated concept with an installed thermal capacity of 450 MW.

Nowadays the nonmoderated reactors are attracting interest because they offer the possibility of transmuting the long-lived actinides produced mostly in light water reactors. The transmutation is most effective in the fast neutron spectrum; however, due to the presence of the fluorine atom in the fuel, partial moderation is maintained, and the neutron spectrum of the MSR is, rather, shifted to the epithermal range. Nevertheless, at this energy, all the minor actinides are fissionable, and the fission-to-capture ratio for these nuclides is still much higher than in the thermal spectrum.[12] Furthermore, the nonmoderated reactor does not require graphite blocks (moderator in the thermal MSR) in the reactor core: they are very susceptible to radiation damage and must be periodically replaced.

At the moment, there are two main directions for the nonmoderated MSR concepts. The first is an actinide burner design based on the Russian MOSART (Molten Salt Actinide Recycler and Transmuter) concept,[6] for which the ^{7}LiF–(NaF)–BeF_2–AnF_3 system is proposed as a fuel salt. The startup and feed material scenarios can include plutonium and minor actinides from pressurized water reactor (PWR) spent fuel. Depending upon the feed material, the fuel salt at equilibrium contains 0.7–1.3 mol% of actinide and lanthanide trifluorides. The second one is an innovative concept called MSFR (molten salt fast reactor), which has been developed by Centre National de la Recherche Scientifique (CNRS) in France.[5,13–16] The fuel in this concept is based on the ^{7}LiF–$^{232}ThF_4$ matrix, with the addition of actinide fluorides as a fissile material. There are two initial fissile choices in the MSFR concept: (1) the ^{233}U-started MSFR and (2) the transuranic-started MSFR with a mix of 87.5% of Pu (^{238}Pu 2.7%, ^{239}Pu 45.9%, ^{240}Pu 21.5%, ^{241}Pu 10.7%, and ^{242}Pu 6.7%), 6.3% Np, 5.3% of Am, and 0.9% of Cm in the form of fluorides, corresponding to the transuranic element composition of a UO_2 fuel after one use in a PWR and 5 years of storage.[17]

One of the very recent MSR designs is the REBUS-3700 concept, which is based on a chloride salt as a fuel. It is a fast breeder reactor proposed by Mourogov and Bokov[11] and it is based on a ^{238}U/^{239}Pu cycle, where ^{238}U serves as a fertile material bred to fissile ^{239}Pu by neutron capture and two consecutive β-decays of ^{239}U and ^{239}Np. Both uranium and plutonium are present in the form of trichlorides dissolved in a matrix of liquid NaCl. In general, the chlorides have higher vapor pressures and lower thermodynamic stability at high temperatures compared to fluorides, but, on the other hand, their melting points are lower. Therefore, more fissile material can be dissolved in the matrix, which is essential for fast breeder reactor designs. However, the chlorides can be used only in fast reactors and not in thermal ones due to the relatively high parasitic neutron capture cross-section of the chlorine atom, as already discussed in **Section 3.13.2.**

A summary of various applications of molten salts in future nuclear reactor designs is given in **Table 2**. As the primary choices for the MSR fuels or coolants are based on the fluoride systems, the chloride systems are not discussed further.

3.13.4 Properties of the MSR Fuels and Coolants

In this section, the physicochemical properties of the primary MSR fuel and coolant choices from **Table 2** are discussed, with the emphasis on the melting behavior, actinide solubility in the fuel matrix, density, viscosity, heat capacity, thermal conductivity, and vapor pressure. All these quantities are highly relevant for the reactor design calculations and a summary of these properties for typical coolant and fuel compositions is given in **Tables 3** and **4** respectively. Optimized phase diagrams of the relevant fluoride systems used as MSR fuels, coolants, or heat transfer salts are also shown in this section.

3.13.4.1 Structural Aspects of Molten Salts

Molten fluoride salts are essentially ionic liquids in which cations and anions form a loose network. Some cations occur in their simplest form, such as Li^+ and Na^+, but some form molecular species like BeF_2, which is a structural analogue to SiO_2, known to be highly associated and forming a network structure that exhibits a glass transition characteristic. In a

Table 2 The various applications of molten salts in nuclear reactor concepts

Reactor type	*Neutron spectrum*	*Application*	*Primary choice*	*Alternative(s)*
MSR breeder	Thermal	Fuel	$^7LiF–BeF_2–AnF_4$	
	Fast	Fuel	$^7LiF–AnF_4$	$^7LiF–CaF_2–AnF_4$, $NaCl–UCl_3–PuCl_3$
		Secondary coolant	$NaF–NaBF_4$	$LiF–BeF_2$, $KF–KBF_4$
MSR burner	Fast	Fuel	$LiF–NaF–BeF_2–AnF_3$	$LiF–NaF–KF–AnF_3$, $LiF–NaF–RbF–AnF_3$
AHTR[a]	Thermal	Primary coolant	$^7LiF–BeF_2$	
VHTR[b]	Thermal	Heat transfer[e]	LiF–NaF–KF	$LiCl–KCl–MgCl_2$
MS-FR[c]	Fast	Primary coolant	$LiCl–NaCl–MgCl_2$	
SFR[d]	Fast	Intermediate coolant[f]	$NaNO_3–KNO_3$	

[a]Advanced high-temperature reactor, graphite-moderated, thermal reactor.
[b]Very high-temperature reactor, graphite-moderated, gas cooled reactor.
[c]Molten salt cooled fast reactor, the solid fuel fast reactor with MS as a coolant.
[d]Sodium cooled fast reactor.
[e]Heat transfer salt is a medium that will be used to deliver heat from the reactor to the hydrogen production plant.
[f]To separate sodium and the steam circuits.

Table 3 Selected properties of the coolant salts

Property	*$LiF–BeF_2$ (0.66–0.34)*	*$NaF–NaBF_4$ (0.08–0.92)*	*LiF–NaF–KF (0.465–0.115–0.42)*
Melting point (K)	728	657 ± 1	727
ρ(kg m^{-3})	2146.3–0.4884T (K)	2446.3–0.711T (K)	2579.3–0.6240T (K)
η(mPa s)	1.81exp(1912.2/T (K))	0.0877exp(2240/T (K))	0.0248exp(4477/T (K))
C_p(J K^{-1} g^{-1})	2.39	1.506	1.88
λ(W m^{-1} K^{-1})	1.1	$0.66–2.37 \times 10^{-4}T$ (K)	$0.36 + 5.6 \times 10^{-4}T$ (K)
$\log_{10}(p$(Pa))	11.914–13003/T (K)	11.638–6550.6/T (K)	10.748–10789/T (K)

Table 4 Selected properties of the fuel salts

Property	*$LiF–ThF_4$ (0.78–0.22)*	*$LiF–BeF_2–ThF_4$ (0.717–0.16–0.123)*	*$LiF–NaF–BeF_2–PuF_3$ (0.203–0.571–0.212–0.013)*
Melting point (K)	841	771	775
ρ(kg m^{-3})	5543.0–1.2500 T (K)	4124.3–0.8690 T (K)	2759.9–0.5730 T (K)
η(mPa s)	0.365exp(2735/T (K))	0.062exp(4636/T (K))	0.100exp(3724/T (K))
C_p(J K^{-1} g^{-1})	1.0	1.55	2.15
λ(W m^{-1} K^{-1})	~1.5[a]	1.5[a]	$0.402 + 0.5 \times 10^{-3}/T$ (K)
$\log_{10}(p$(Pa))	11.902–12 989/T (K)	11.158–10 790.5/T (K)	11.6509–12 827/T (K)

[a]Value for $T = 1023$ K.

recent study by Salanne *et al.*,[18] a molecular dynamic study was performed on the $LiF–BeF_2$ system in order to understand the structure of the $(Li,Be)F_{2-x}$ melt. Figure 2 shows the distribution of various species observed in the solution as a function of BeF_2 composition. At low concentrations of BeF_2 in LiF, the mixture behaves as a well-dissociated ionic melt consisting of Li^+, BeF_4^{2-}, and F^- species. As BeF_2 concentration increases, the BeF_4^{2-} units start to bond together sharing a common F^- ion, first creating $Be_2F_7^{3-}$ species, followed by $Be_3F_{10}^{7-}$ species, and so forth, resulting in a polymer of several BeF_4^{2-} units. This polymerization is also a reason why the viscosity of pure BeF_2 is much higher compared to that of other fluorides discussed in this chapter. BeF_4^{2-} species were also experimentally observed by spectroscopic studies, as reported by Toth and Gilpatrick.[19] Lanthanide fluorides, ThF_4 or PuF_3 also form molecular species in their liquid form, but in comparison to BeF_2, they do not exhibit polymerization. Dracopolous *et al.*[20,21] investigated the structure of molten $KF–YF_3$ and $KF–LnF_3$

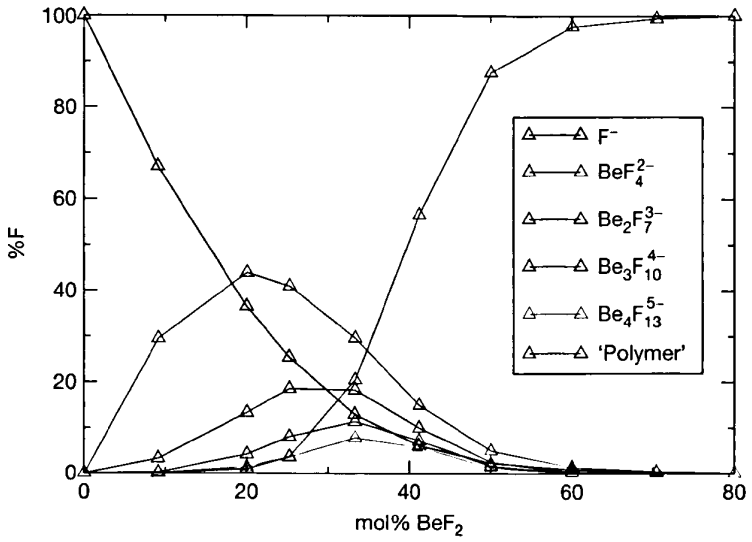

Figure 2 Percentage of F atoms involved in various species observed in the LiF–BeF_2 system as a function of composition; 'polymer' means a cluster with a Be nuclearity >4, whereas F^- implies that the ion is coordinated only to Li^+. Reproduced from Salanne, M.; Simon, C.; Turq, P. *J. Phys. Chem. B* **2007**, *111*, 4678–4684.

(Ln = La, Ce, Nd, Sm, Dy, Yb) systems using Raman spectroscopy and found that at $x(LnF_3) \leq 0.25$, LnF_6^{3-} are the predominant species surrounded by K^+ cations. At higher concentrations of LnF_3, the lanthanides are forced to share common fluorides and start to create loose structures of bridged octahedra. On the basis of these two studies, the authors concluded that lanthanide melts have similar structural behavior. In case of thorium, a tetravalent ion is the only known species in molten fluorides. As reported by Barton,[22] ThF_4 forms mainly anionic complexes of the general formula ThF_{4+m}^{m-}, and the existence of ThF_5^- is claimed.[23] In case of uranium, tri- or tetravalent ions are stable in the molten fluoride salt. It has been demonstrated[19] that UF_4 dissolves in the fluoride melts, forming complexes of coordination numbers 7 or 8. It has been shown that in fluoride-rich systems, the UF_8^{4-} species predominates, while with the reduction of fluoride ions, the UF_7^{3-} species is produced according to $UF_8^{4-} \rightleftharpoons UF_7^{3-} + F^-$. Furthermore, the same authors confirmed that approximately equal amounts of UF_8^{4-} and UF_7^{3-} occur in the LiF–BeF_2 melt of intermediate composition.

3.13.4.2 Phase Diagrams

3.13.4.2.1 LiF–BeF_2

The LiF–BeF_2 phase diagram has been assessed by van der Meer *et al.*[24] and more recently by Beneš and Konings,[25] the latter version being preferred as the authors considered not only the equilibrium points measured,[26–28] but also the mixing enthalpies of the (Li,Be)F_x liquid solution measured by Holm and Kleppa.[29] The LiF–BeF_2 phase diagram is shown in **Figure 3**; it is characterized by two eutectic invariant equilibria found at $T = 636$ K and $x(BeF_2) = 0.517$, and $T = 729$ K and $x(BeF_2) = 0.328$ in the calculation. Two intermediate phases, Li_2BeF_4 and $LiBeF_3$, are present in the system as well, the first melting congruently at $T = 729$ K, whereas the latter decomposes below the solidus at $T = 557$ K. A miscibility gap appears in the BeF_2-rich side, with the monotectic temperature found at $T = 772$ K, while the critical temperature was found at $T_c = 812$ K and $x(BeF_2) = 0.826$.

3.13.4.2.2 LiF–PuF_3

The thermodynamic assessment of the LiF–PuF_3 system was made in a study by van der Meer *et al.*[30] and later by Beneš and Konings,[31] using a different thermodynamic model based on the equilibrium data measured by Barton and Strehlow.[32] The calculated phase diagram as obtained from the data of Beneš and Konings is shown in **Figure 4**, indicating very good agreement with the experimental data. The system is characterized by a single eutectic at $T = 1018$ K and $x(PuF_3) = 0.212$.

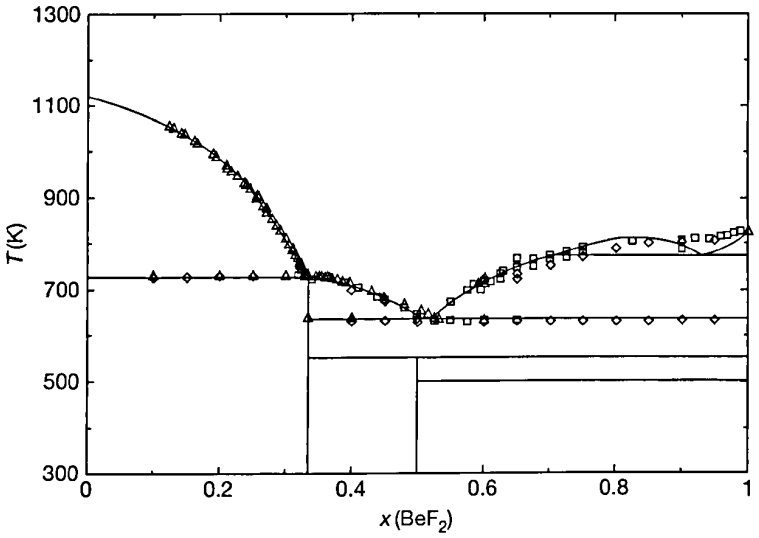

Figure 3 Calculated LiF–BeF_2 phase diagram from Beneš and Konings[25]: ◇ experimental data by Roy *et al.*[26]; □ data by Thoma *et al.*[27]; and △ data by Romberger *et al.*[28] Reproduced from Beneš, O.; Konings, R. J. M. *J. Chem. Thermodyn.* **2009**, *41*, 1086–1095.

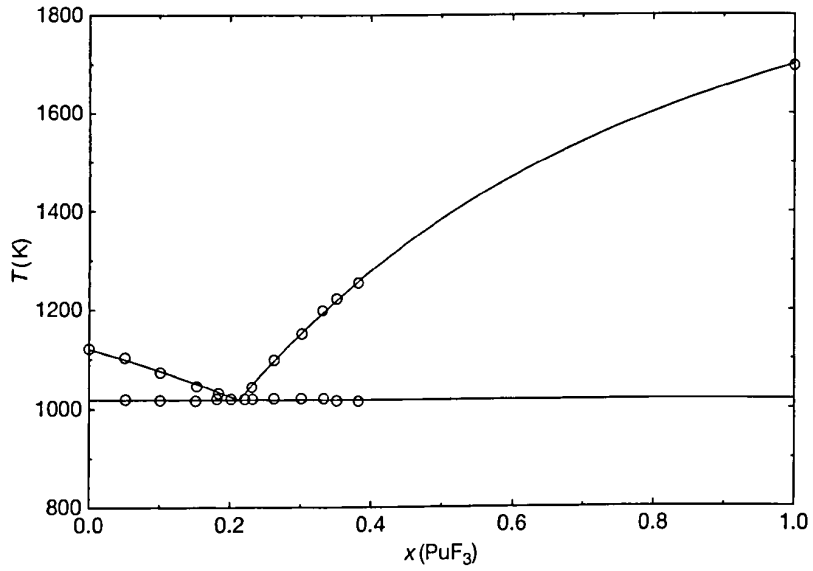

Figure 4 The calculated LiF–PuF_3 phase diagram based on the thermodynamic data taken from Beneš and Konings[31]: ○ experimental data measured by Barton and Strehlow.[32] Reproduced from Beneš, O.; Konings, R. J. M. *J. Nucl. Mater.* **2008**, *377*(3), 449–457.

3.13.4.2.3 NaF–PuF_3

Similar to the LiF–PuF_3 system, the NaF–PuF_3 phase diagram has been thermodynamically assessed in two studies,[30,31] both based on the experimental data measured by Barton *et al.*[33] The phase diagram is shown in Figure 5 and is characterized by one eutectic at $T = 999$ K and $x(PuF_3) = 0.221$ and one peritectic at $T = 1111$ K and $x(PuF_3) = 0.387$, where the $NaPuF_4$ intermediate compound decomposes.

3.13.4.2.4 BeF_2–PuF_3

To our best knowledge, there are no published experimental data on the BeF_2–PuF_3 system. Beneš and Konings[25] made a thermodynamic assessment of this

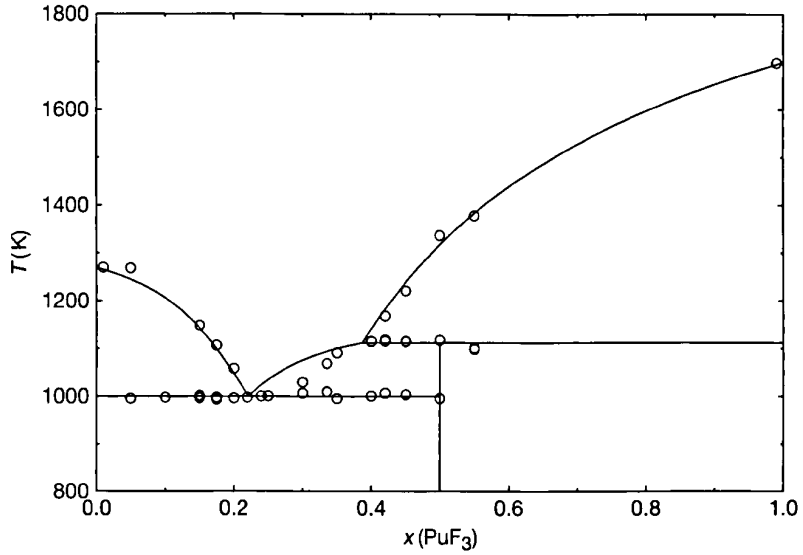

Figure 5 The calculated $NaF–PuF_3$ phase diagram based on the thermodynamic data taken from Beneš and Konings[31]: o experimental data measured by Barton *et al.*[33] Reproduced from Beneš, O.; Konings, R. J. M. *J. Nucl. Mater.* **2008**, *377*(3), 449–457.

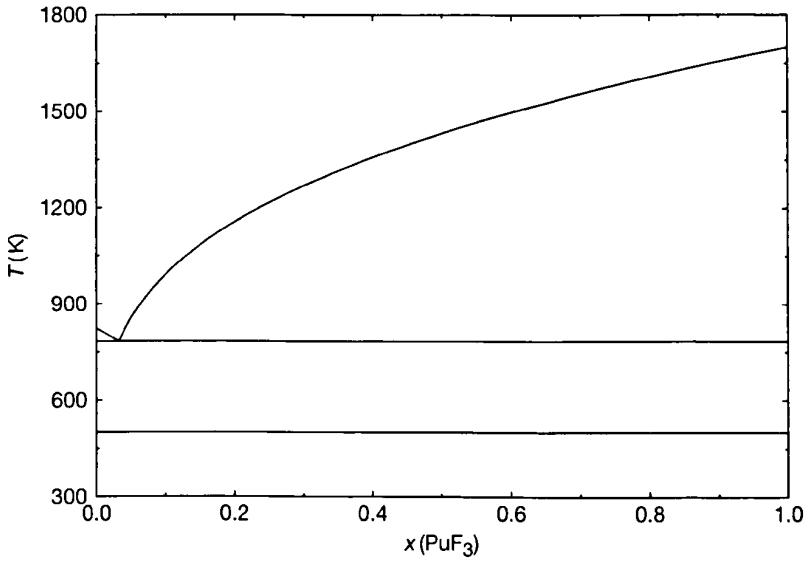

Figure 6 The estimated $BeF_2–PuF_3$ phase diagram. Reproduced from Beneš, O.; Konings, R. J. M. *J. Chem. Thermodyn.* **2009**, *41*, 1086–1095.

system, assuming an ideal behavior of the liquid phase. The estimated $BeF_2–PuF_3$ phase diagram is shown in **Figure 6**, consisting of a single eutectic point at $T = 783$ K and $x(PuF_3) = 0.031$.

3.13.4.2.5 BeF_2–ThF_4

The $BeF_2–ThF_4$ system was assessed by van der Meer *et al.*[24] using the equilibrium data measured by Thoma *et al.*[34] The calculated phase diagram is shown in **Figure 7**. It is a simple eutectic system with the eutectic at $T = 800$ K and $x(ThF_4) = 0.019$.

3.13.4.2.6 LiF–AnF_4

The $LiF–ThF_4$ system is a reference salt for the MSFR concept. The equilibrium diagram of the $LiF–ThF_4$ system was reported by Thoma *et al.*[35] on the

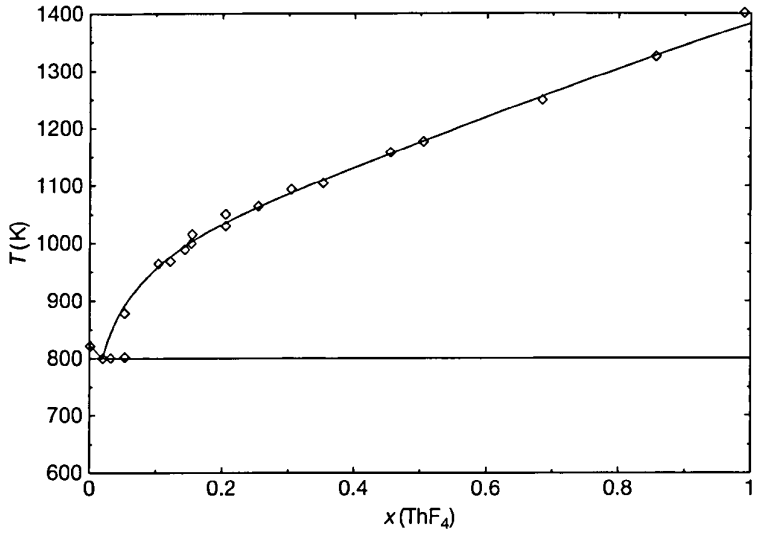

Figure 7 The calculated BeF_2–ThF_4 phase diagram. Reproduced from van der Meer, J.; Konings, R. J. M.; Jacobs, M. H. G.; Oonk, H. A. J. *J. Nucl. Mater.* **2005**, *344*, 94–99.

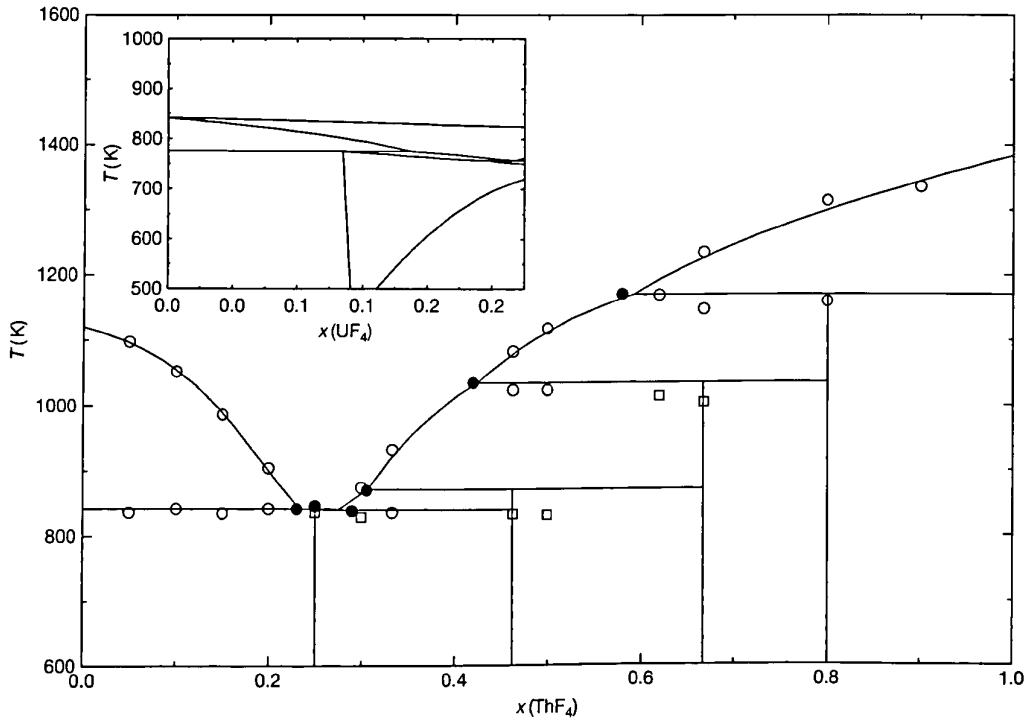

Figure 8 The equilibrium diagram of the LiF–ThF_4 system assessed in Beneš *et al.*[49]: ○ thermal analysis data obtained by Thoma *et al.*[35]; □ supercooled data; • invariant equilibria as reported in Thoma *et al.*[35] Inset: calculated ThF_4–UF_4 pseudobinary system with constant amount of LiF at 78 mol%. Reproduced from Beneš, O.; Beilmann, M.; Konings, R. J. M. *J. Nucl. Mater.* **2010**, *405*, 186–198.

basis of thermal analysis and thermal quenching. Based on their data, the phase diagram was thermodynamically assessed by van der Meer *et al.*[24] and more recently by Beneš *et al.*[49] The phase diagram from the latter study,[24] is shown in **Figure 8**. The LiF–ThF_4 phase diagram consists of four mixed compounds: Li_3ThF_7, which melts congruently and $Li_7Th_6F_{31}$, $LiTh_2F_9$, and $LiTh_4F_{17}$, all melting peritectically. Two eutectic points

were found at $x_{eut_1} = (22.4 \pm 1)$mol% ThF_4 with $T_{eut_1} = (841 \pm 1)$K, and $x_{eut_2} = (28.3 \pm 1)$mol% ThF_4 with $T_{eut_2} = (838 \pm 1)$K, the first selected as a fuel composition of the MSFR concept.

In this notation, AnF_4 is represented mainly by ThF_4, which serves as a fertile material, and by UF_4, which is the fissile material, normally presented with a concentration of up to 4 mol%. As UF_4 and ThF_4 form close-to-ideal solid and liquid solutions, the melting point of the fuel is only slightly affected by the UF_4/ThF_4 substitution. The effect of UF_4 addition is demonstrated in the inset graph of **Figure 8**, which shows the calculated liquidus line (the very upper line) of the ThF_4–UF_4 pseudobinary system with the amount of LiF constant at 78 mol%. The left axis of the graph corresponds to the proposed LiF–ThF_4 (78–22 mol%) fuel composition (eutectic$_1$ of the LiF–ThF_4 system) and the right axis corresponds to the LiF–UF_4 (78–22 mol%) composition; thus, in this case, all ThF_4 is substituted by UF_4. As can be seen from the figure, the liquidus line along this section is nearly constant, with a total drop of only 18 K.

3.13.4.2.7 LiF–BeF_2–AnF_4

The LiF–BeF_2–ThF_4 system is the reference salt for a MSR designed as a thermal breeder. The equilibrium diagram of this system was measured by Thoma *et al.*[34] It contains a single eutectic at 1.5 mol% ThF_4 and $T_{eut} = (629 \pm 3)$K; no ternary compounds were found. van der Meer *et al.*[36] calculated the ternary from the assessed binaries and found good agreement with the experimental diagram. The calculated phase diagram of the LiF–BeF_2–ThF_4 system is shown in **Figure 9**, as a projection of the liquidus surface.

In the MSBR concept, the proposed fuel composition in the LiF–BeF_2–AnF_4 system was 71.7–16.0–12.3, where the AnF_4 fraction was made up of 12.0 mol% ThF_4 and 0.3 mol% UF_4. In this section, AnF_4 is represented by pure ThF_4, which is possible for the same reasons as discussed in **Section 3.13.3.1.1**. If we then assume that the concentration of ThF_4 must be 12.3 mol%, it is possible, according to thermodynamic data, to determine the lowest melting temperature of such a system and its exact composition. It has been found at $T = 786$ K and LiF–BeF_2–ThF_4 (67.1–20.6–12.3 mol%) (Composition 1), thus reasonably close to the data of the MSBR fuel ($T = 771$ K and LiF–BeF_2–AnF_4 (71.7–16.0–12.3 mol%) (Composition 2)). This means that, keeping the safety margin of 50 K, the inlet temperature of the reactor must be a minimum of 836 K. This is a promising result because it is lower than the inlet temperature in MSBR, which was found to be 839 K, as discussed in **Section 3.13.1**. According to the modeled phase diagram (**Figure 9**),

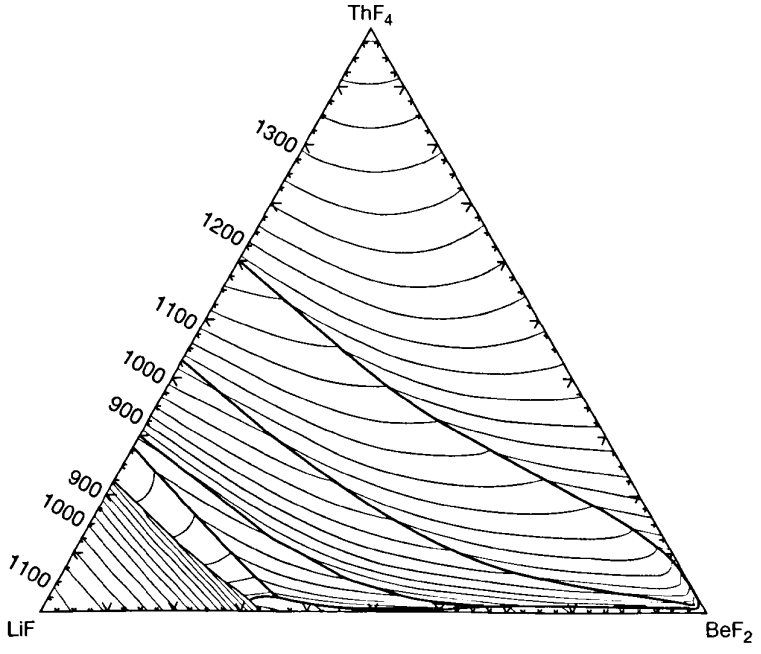

Figure 9 Calculated liquid surface of the LiF–BeF_2–ThF_4 phase diagram. Isotherms are labeled in K with interval of 25 K. Reproduced from van der Meer, J.; Konings, R. J. M.; Oonk, H. A. J. *J. Nucl. Mater.* **2006**, *357*, 48–57.

the calculated liquidus temperature of the MSBR composition (Composition 2) is 795 K.

As the melting temperatures of Compositions 1 and 2 are very close, we focus (see **Table 4**) the discussion only on the preferred composition of the MSBR concept ($LiF–BeF_2–ThF_4$ (71.7–16.0–12.3 mol%) (Composition 2)). This salt has also been more extensively studied, and thus more of its properties are known.

3.13.4.2.8 *LiF–NaF–BeF_2–AnF_3*

The $LiF–NaF–BeF_2–PuF_3$ system is a reference salt in the MOSART concept. The full thermodynamic description of this quaternary system has been assessed in a recent study by Beneš and Konings,[25] using the solubility data of PuF_3 measured by Barton,[37] Mailen *et al.*,[38] and Ignatiev *et al.*[39,40] for the optimization of the PuF_3-containing ternary subsystems. Based on this work,[25] the optimized fuel composition is $LiF–NaF–BeF_2–PuF_3$ (20.3–57.2–21.2–1.3), which is exactly the point that corresponds to the lowest eutectic in the $LiF–NaF–BeF_2–PuF_3$ system, with a fixed concentration of PuF_3 at 1.3 mol% as an equilibrium concentration of AnF_3 after 10 years of operation of the MOSART reactor.[41] Note here that, in order to simplify the study, all actinides were represented by plutonium. This was possible as plutonium is the major constituent of all actinides considered in the MOSART fuel. A pseudoternary phase diagram of the $LiF–NaF–BeF_2–(PuF_3 = 1.3$ mol%) system is shown in **Figure 10**. The melting temperature of the lowest eutectic composition is calculated at 775 K, which is much lower than the designed inlet temperature of the MOSART concept[6] and therefore acceptable for reactor purposes.

The optimized fuel composition as found in Beneš and Konings[25] varies slightly from that of the MOSART concept ($LiF–NaF–BeF_2–PuF_3$ (14.8–57.4–26.5–1.3)). Because the authors of the MOSART concept did not have a full thermodynamic description of the whole $LiF–NaF–BeF_2–PuF_3$ system, they took the eutectic of the $LiF–NaF–BeF_2$ system with the lowest BeF_2 content, as reported in Thoma,[42] and directly dissolved 1.3 mol% of AnF_3 in it. Hence, they did not consider the shift of the eutectic composition while adding AnF_3, which was demonstrated in Beneš and Konings.[25]

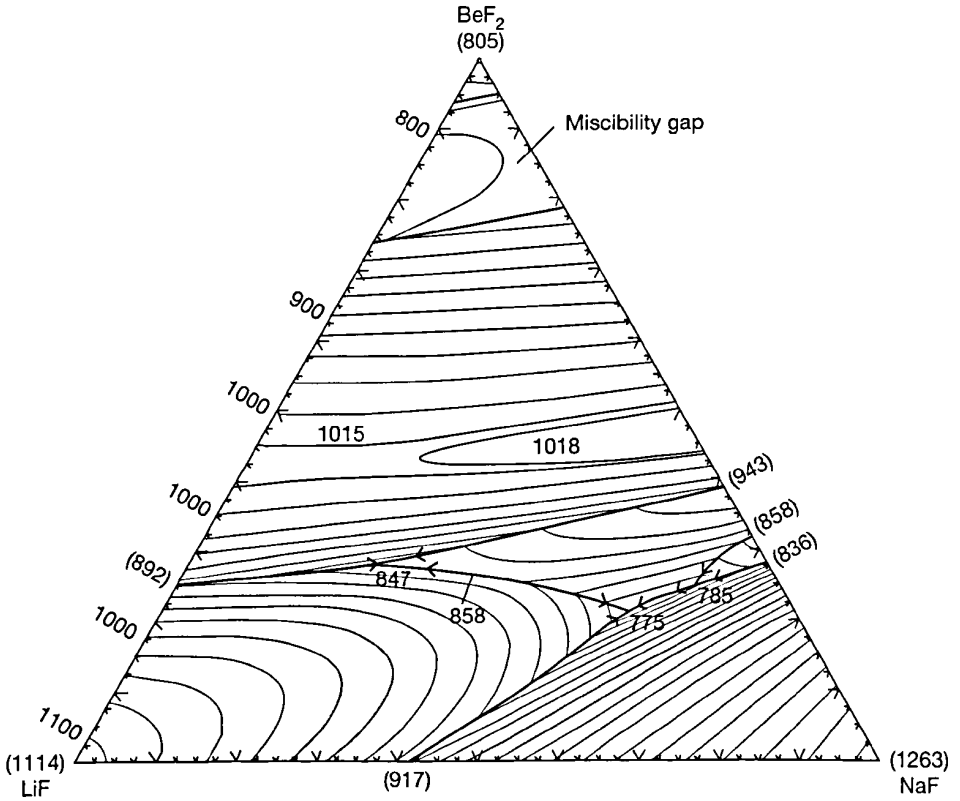

Figure 10 Calculated pseudoternary phase diagrams of the $LiF–NaF–BeF_2$ system with constant amount of $PuF_3 = 1.3$ mol%. Reproduced from Beneš, O.; Konings, R. J. M. *J. Fluor. Chem.* **2009**, *130*, 22–29.

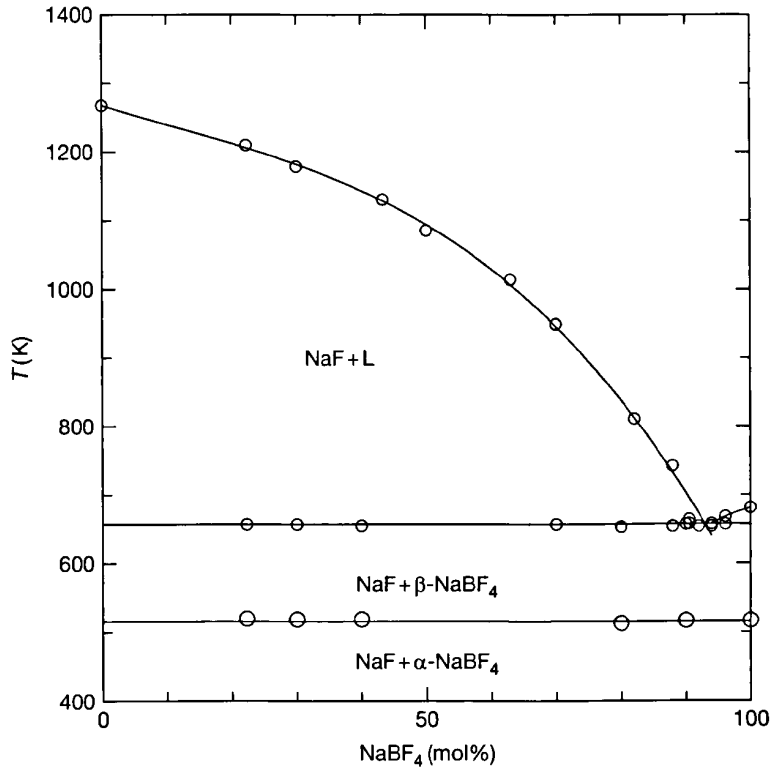

Figure 11 The equilibrium diagram of the NaF–$NaBF_4$ system. Reproduced from Beneš, O.; Konings, R. J. M. *J. Fluor. Chem.* **2009**, *130*, 22–29.

3.13.4.2.9 NaF–$NaBF_4$

The equilibrium diagram of the NaF–$NaBF_4$ system was studied by Selivanov and Stender,[43] and Barton *et al.*[44] Both studies indicate that it is a simple eutectic system, but the eutectic temperatures and compositions differ considerably. In view of their more careful sample preparation, the results of Barton *et al.* are preferred, and this diagram is shown in **Figure 11**. They found $x_{eut} = (92 \pm 1)$ mol% $NaBF_4$ with $T_{eut} = (657 \pm 1)$ K.

3.13.4.2.10 LiF–NaF–KF

A eutectic mixture of LiF, NaF, and KF is one of the possible candidates as an intermediate heat transfer salt used to deliver the heat from the high-temperature reactor (advanced high-temperature reactor (AHTR) or very high-temperature reactor (VHTR)) to, for example, a hydrogen production plant. Alternatively, the LiF–NaF–KF mixture can be considered as a solvent for actinide trifluorides in the molten salt actinide burner concept.

The LiF–NaF–KF phase diagram was measured by Bergmann and Dergunov,[45] who found the ternary eutectic with the lowest melting point at $T = 727$ K and LiF–NaF–KF (46.5–11.5–42.0 mol%). Thermodynamic assessment of this system was done in several studies,[46–48] all of which were in close agreement. **Figure 12** shows the LiF–NaF–KF phase diagram calculated using the data from the study by Beneš and Konings,[48] who found the ternary eutectic at $T = 726$ K and LiF–NaF–KF (45.3–13.2–41.5 mol%).

3.13.4.3 Solubility of Actinides in the Fluoride Melt

3.13.4.3.1 ThF_4 in molten LiF

The solubility of ThF_4 in a matrix of LiF can be deduced from the binary phase diagram in **Figure 8**. For example, the solubility of ThF_4 in a melt of LiF for $T = 903$ K (inlet temperature of the MSFR) is between 20.0 and 32.3 mol%. Compositions in this range are, thus, of interest as fuel for the MSFR. In practice, the LiF–ThF_4 (78–22 mol%) composition is the prime choice.

3.13.4.3.2 ThF_4 in molten LiF–BeF_2

The solubility of ThF_4 in the LiF–BeF_2 matrix has been calculated for $T = 839$ K (inlet temperature

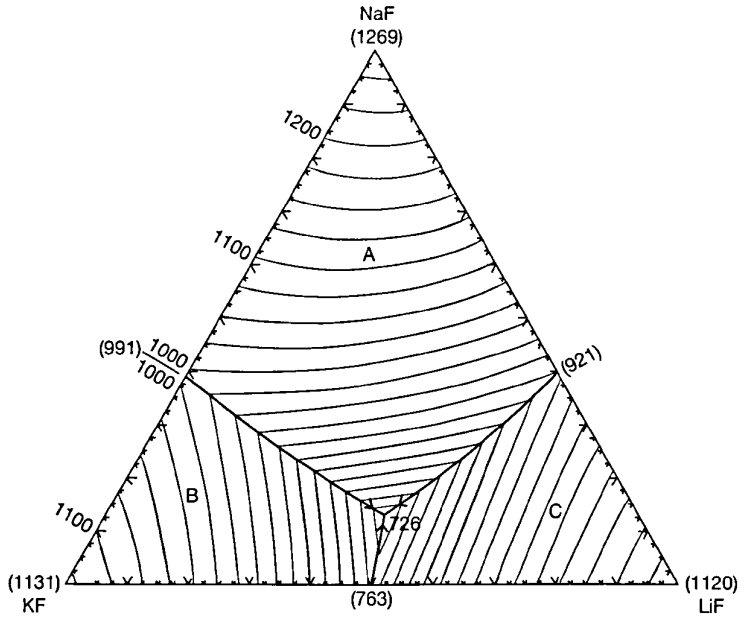

Figure 12 Calculated liquid surface of the LiF–NaF–KF phase diagram. Isotherms are labeled in K with interval of 25 K. Primary phase fields: (A) (Li,Na,K)F; (B) (Na,K)F; (C) (Li,Na)F. Reproduced from Beneš, O.; Konings, R. J. M. *J. Fluor. Chem.* **2009**, *130*, 22–29.

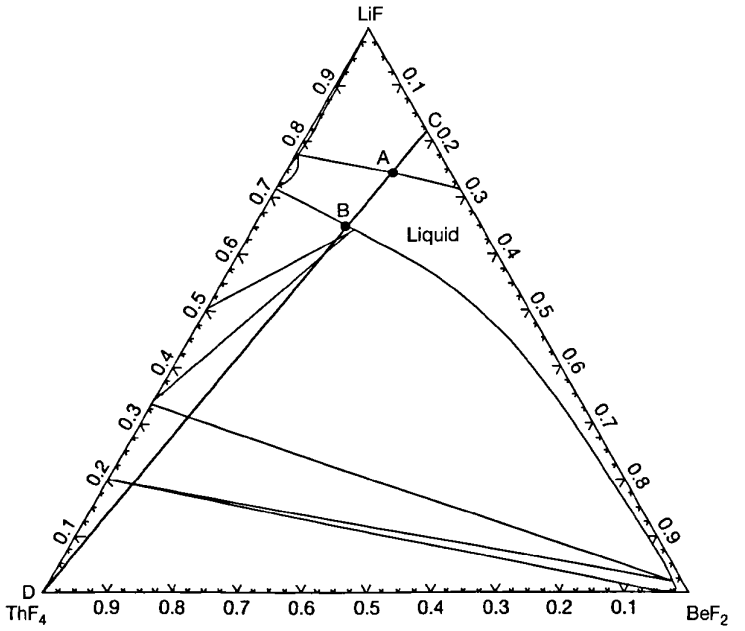

Figure 13 Isothermal plot of the LiF–BeF_2–ThF_4 phase diagram at $T = 839$ K. Reproduced from Beneš, O.; Konings, R. J. M. *J. Fluor. Chem.* **2009**, *130*, 22–29.

of MSBR), keeping a constant ratio of $LiF/BeF_2 = 0.818/0.182$. This ratio corresponds to the fuel composition proposed in MSBR. **Figure 13** shows the ternary phase diagram of the LiF–BeF_2–ThF_4 system at $T = 839$ K. The straight bold line represents the LiF/BeF_2 ratio at 0.818/0.182 within the whole field of the diagram, while the ThF_4 concentration varies from 0 to 100 mol% as it moves from point 'C'

towards 'D.' The solubility of ThF_4 in the LiF–BeF_2 matrix thus derived is between 9.2 and 20.8 mol%. The interval of the solubility is represented by the 'A' and 'B' signs, respectively, which correspond to the intersection of the 'CD' line with the surface of the liquid field.

3.13.4.3.3 UF_4 in molten LiF–ThF_4

To our best knowledge, there are no experimental data of the UF_4 solubility in the LiF–ThF_4 binary matrix. However, based on the thermodynamic assessment of the LiF–NaF–ThF_4–UF_4 system,[49] the solubility of UF_4 in the LiF–ThF_4 (78–22) composition (primary fuel choice of the MSFR concept) has been calculated for a temperature range of 840–880 K giving:

$$\log_{10}\mathcal{Q}(\text{mol\%}) = 42.7475 - 0.1052T(\text{K}) + 6.6086 \times 10^{-5}T^2(\text{K}) \quad [1]$$

3.13.4.3.4 PuF_3 in molten LiF–BeF_2

The solubility of PuF_3 in the LiF–BeF_2 binary melt has been measured by Barton[22] and Mailen *et al.*[38] Barton measured the PuF_3 solubility in LiF–BeF_2 (71.3–28.7) and LiF–BeF_2 (63–37) compositions for the temperature range of 736–927 K, whereas Mailen *et al.* measured the PuF_3 solubility in LiF–BeF_2 (67–33) composition for the temperature range of 59–657 K. Furthermore, Barton measured the PuF_3 solubility at $T = 838$ K in the LiF–BeF_2 matrix as a function of composition from $x(\text{LiF}) = 0.52$ to 0.72. Beneš and Konings[25] recently evaluated the LiF–NaF–BeF_2–PuF_3 system thermodynamically and found very good agreement with all experimentally determined solubility data by Barton and Mailen *et al.* On the basis of their assessment, the PuF_3 solubility in the LiF–BeF_2 (67–33) composition has been calculated for the temperature range of 780–930 K, giving:

$$\log_{10}\mathcal{Q}(\text{mol\%}) = -4.0975 + 4.32 \times 10^{-3}T(\text{K}) \quad [2]$$

3.13.4.3.5 PuF_3 in molten LiF–NaF–BeF_2

According to the thermodynamic model of the LiF–NaF–BeF_2–PuF_3 system published in Beneš and Konings,[25] the solubility of PuF_3 in the recommended fuel matrix composition (LiF–NaF–BeF_2 (20.6–57.9–21.5)) was calculated for the temperature range of 823–973 K and fitted with the polynomial equation below:

$$\log_{10}\mathcal{Q}(\text{mol\%}) = -5.3526 + 9.7386 \times 10^{-3}T(\text{K}) - 3.4105 \times 10^{-6}T^2(\text{K}) \quad [3]$$

Based on this equation, the total PuF_3 solubility in the LiF–NaF–BeF_2 (20.6–57.9–21.5) melt at the inlet temperature of the MOSART reactor concept ($T = 873$ K) is 3.55 mol%. This value is slightly higher than the measured value in the MOSART matrix composition (LiF–NaF–BeF_2 (15–58–27)), which was determined to be 3.08 mol%.[6] Higher solubility was achieved in the former case because of the lower content of BeF_2, which is the main fuel component responsible for low AnF_3 solubility, as discussed in Beneš and Konings.[25]

3.13.4.3.6 PuF_3 in molten LiF–BeF_2–ThF_4

The solubility of PuF_3 in various compositions of LiF–ThF_4 and LiF–BeF_2–ThF_4 melts were measured by Sood *et al.*,[50] between 783 and 1060 K. Results of their measurements are reported in **Table 5**,

Table 5 Solubility of PuF_3 in the LiF–BeF_2–ThF_4 melts measured by Sood *et al.*[50]

Salt composition (mol%)			*Temperature range (K)*	*A*	*$-B \times 10^{-3}$*
LiF	*BeF_2*	*ThF_4*			
74.0	22.1	3.9	851–1021	3.55 ± 0.14	2.97 ± 0.14
76.9	17.1	6.0	878–973	3.49 ± 0.23	2.82 ± 0.21
75.3	16.7	8.0	812–1029	3.80 ± 0.05	3.13 ± 0.04
68.2	20.5	11.3	821–1049	2.98 ± 0.05	2.52 ± 0.06
71.6	16.2	12.2	796–1031	2.95 ± 0.07	2.46 ± 0.07
71.3	15.5	13.2	783–1060	2.62 ± 0.07	2.15 ± 0.06
70.0	14.0	16.0	802–949	2.56 ± 0.11	2.06 ± 0.10
75.0	5.0	20.0	826–1038	2.57 ± 0.14	1.84 ± 0.13
80.0	0.0	20.0	926–1054	2.62 ± 0.19	1.78 ± 0.19
75.0	0.0	25.0	882–1038	2.58 ± 0.05	1.76 ± 0.05
70.0	0.0	30.0	873–1018	2.84 ± 0.07	1.99 ± 0.07
65.0	0.0	35.0	935–1026	3.01 ± 0.08	2.20 ± 0.08

showing the derived coefficients for the general equation:

$$\log_{10}\mathcal{Q}(\text{mol\%}) = A + B/T(\text{K}) \quad [4]$$

3.13.4.4 Density and Viscosity

3.13.4.4.1 LiF–BeF_2

The density of liquid LiF–BeF_2 has been measured by Blanke *et al.*[51] from 0 to 55 mol% BeF_2, by Cantor *et al.*[52] for 50.2, 74.9, and 89.2 mol% BeF_2, and by Cantor[53] for the 34 mol% BeF_2 composition. As discussed by van der Meer *et al.*,[36] the molar volumes derived from the measured density data indicate ideal behavior, suggesting that the density can be interpolated from the molar volume data for the pure components. However, the density and molar volume of liquid BeF_2 are known only at a single temperature (T= 1073 K), and not at all as a function of temperature. Therefore, we have selected the results of the 66:34 composition from Cantor[53]:

$$\rho(\text{kg m}^{-3}) = 2146.3 - 0.4884T(\text{K}) \quad [5]$$

The viscosity of liquid LiF–BeF_2 has been measured by Cohen and Jones[54] and Abe *et al.*[55] for the compositions 31and 32.8 mol% BeF_2, respectively, as well as by Blanke *et al.*,[51] Cantor *et al.*,[52] and Desyatnik *et al.*[56] for a wide(r) range of compositions and temperatures.

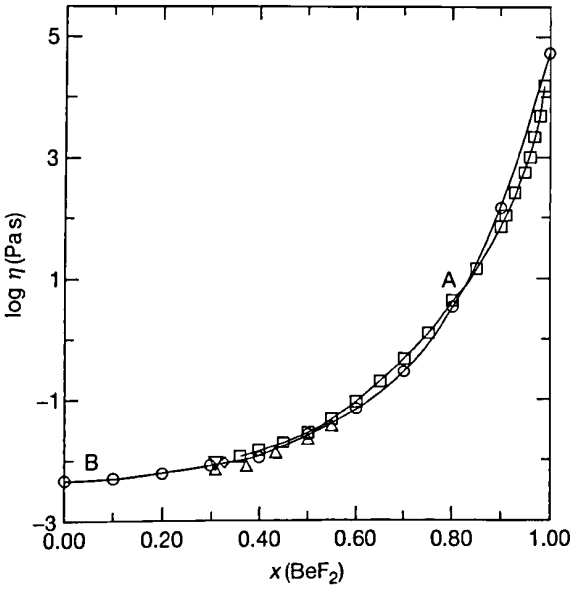

Figure 14 The viscosity of liquid LiF–BeF_2 at 873 K: ▽ Cohen and Jones[54]; △ Blanke *et al.*[51]; □ (curve A), Cantor *et al.*[52]; ○ (curve B), Desyatnik *et al.*[56]; ◇ Abe *et al.*[55] Reproduced from Beneš, O.; Konings, R. J. M. *J. Fluor. Chem.* **2009**, *130*, 22–29.

The agreement between the studies is excellent, as shown in **Figure 14** in an isothermal section at 873 K. From the results, we interpolate for the 66–34 composition:

$$\eta(\text{mPa s}) = 0.116\exp(3755/T(\text{K})) \quad [6]$$

3.13.4.4.2 LiF–AnF_4

The density of LiF–ThF_4 mixtures was measured by Porter and Meaker[57] and Hill *et al.*[58] The data are in good agreement and clearly indicate a linear dependence of the molar volume on composition as shown in **Figure 15**, confirming ideal behavior. The density of the 78–22 composition as measured by Porter and Meaker,[57] is given by:

$$\rho(\text{kg m}^{-3}) = 5543 - 1.25T(\text{K}) \quad [7]$$

The density of liquid LiF–UF_4 mixtures were measured by Blanke *et al.*[51] and Porter and Meaker.[57] The results are in excellent agreement, as shown in **Figure 15**. The results indicate a linear dependence of the molar volume on composition, confirming ideal behavior.

The viscosity of LiF–ThF_4 mixtures was measured by Chervinskij *et al.*[59] from 0 to 100 mol% ThF_4. The results reveal a strong deviation from ideal behavior around the eutectic composition. An isothermal section in **Figure 15** shows a steady increase from LiF to ThF_4. The viscosity of the 78–22 composition interpolated from the results is given by:

$$\eta(\text{mPa s}) = 0.365\exp(2735/T(\text{K})) \quad [8]$$

The viscosity of the LiF–UF_4 system measured by the same group[60] shows a less strong increase with the AnF_4 content compared to ThF_4 (**Figure 15**). As a result, the above equation probably overestimates the viscosity slightly in the case of part replacement of ThF_4 by UF_4.

3.13.4.4.3 LiF–BeF_2–ThF_4

The densities of the three compositions of the LiF–BeF_2–ThF_4 system, with almost constant LiF concentration, were measured by Cantor.[53] Unfortunately, the density of the LiF–BeF_2–ThF_4 (71.7–16.0–12.3) composition has not been measured; however, a very close composition (LiF–BeF_2–ThF_4 (70.06–17.96–11.98)) has been determined and the corresponding density function is given below:

$$\rho(\text{kg m}^{-3}) = 4043.9 - 0.8064T(\text{K}) \quad [9]$$

It has been shown by van der Meer and Konings[61] that the molar volumes and thus the densities of all three

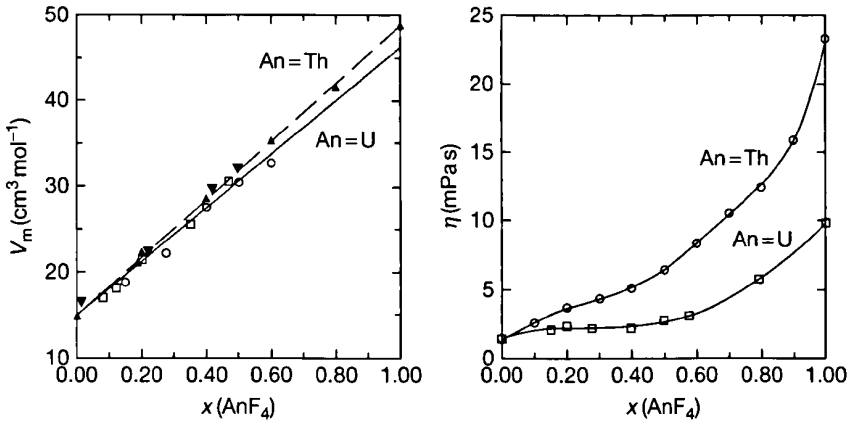

Figure 15 The molar volume (left) and viscosity (right) of liquid LiF–ThF_4 and LiF–UF_4 at 1273 K. Right figure: ○ data by Chervinskij *et al.*[59]; □ data by Desyatnik *et al.*[60]; Left figure: ▲ data by Hill *et al.*[58]; ▼ data by Porter and Meaker[57]; □ data by Blanke *et al.*[51]; ○ data by Porter and Meaker.[57] Reproduced from Beneš, O.; Konings, R. J. M. *J. Fluor. Chem.* **2009**, *130*, 22–29.

LiF–BeF_2–ThF_4 compositions measured in Cantor[53] behave almost ideally. Based on this triplet of data and with the assumption of the ideality, it is possible to estimate the density function of temperature of pure BeF_2, which has not been measured yet. The density of liquid BeF_2 was measured by Mackenzie,[62] but only at 1073 K, obtaining the value of $1947 \pm 10\,kg\,m^{-3}$. Cantor *et al.*[52] also measured the density, but, due to the experimental difficulties, they derived only an approximate value: $1960\,kg\,m^{-3}$ at 1123 K. The value of MacKenzie is recommended and taken as a constraint in our estimation. The obtained density for liquid BeF_2 as a function of temperature is shown below:

$$\rho(kg\,m^{-3}) = 3190.5 - 1.1589T(K) \qquad [10]$$

Using eqn [10] together with the selected data for the LiF and ThF_4 densities taken from van der Meer and Konings,[61] we have calculated the expected density function of temperature for the LiF–BeF_2–ThF_4 (71.7–16.0–12.3 mol%) composition (MSBR). The obtained equation is given below:

$$\rho(kg\,m^{-3}) = 4124.3 - 0.8690T(K) \qquad [11]$$

The results from eqns [9] and [11] agree very well. As the former equation is based on the experimental results whereas the latter is an estimate, and both equations refer to very similar compositions, the extrapolation of the density in the LiF–BeF_2–ThF_4 system can be justified on the basis of ideal behavior. Based on eqn [11], the density of the salt mixture at $T = 973$ K is $3279\,kg\,m^{-3}$, for the LiF–BeF_2–ThF_4–UF_4 (71.0–16.0–12.0–1.0 mol%) composition, while the reported density at the same temperature taken from the study by Briant and Weinberg[63] is $3250\,kg\,m^{-3}$: values that are in close agreement.

The viscosity of liquid LiF–BeF_2–ThF_4 of two compositions was measured by Cantor.[53] The viscosity of the quaternary LiF–BeF_2–ThF_4–UF_4 (71–16–12–1) composition, which is nearly identical to our reference selection (LiF–BeF_2–ThF_4 (71.7–16–12.3)), has been reported in Powers *et al.*[64] for the temperature range of 873–1073 K, giving:

$$\eta(mPa\,s) = 0.062\exp(4636/T(K)) \qquad [12]$$

3.13.4.4.4 LiF–NaF–BeF_2–AnF_4

Densities of several LiF–NaF–BeF_2 mixtures have been measured in various studies,[6,64] but the exact compositions are different from that of our recommended fuel choice from **Table 3**. However, in a recent study by Khokhlov *et al.*[65] the density of a very similar ternary mixture (LiF–NaF–BeF_2 (22–56.7–21.3 mol%)) was estimated, using an additive law of molar volumes according to the equation $V = \sum N_i V_i$, where V_i is a molar volume of LiF and NaF end members, and LiF–BeF_2 and NaF–BeF_2 mixtures, whose compositions are shown in square brackets in the following notations: [0.508LiF–0492BeF_2]–0.567NaF; [0.727NaF–0.273BeF_2]–0.22LiF. The density of the ternary mixture was taken as a mean value from these two notations, and the temperature function thus derived is shown below:

$$\rho(g\,cm^{-3}) = 2.5777 - 5.38 \times 10^{-4}T(K) \qquad [13]$$

Densities of binary $LiF–BeF_2$ and $NaF–BeF_2$ mixtures were measured as a function of temperature and composition and taken from the work of Janz[66] as reported in Khokhlov *et al.*[65] Khokhlov *et al.* also made calculations for the same compositions as measured by Zherebtsov and Ignatiev[6] ($LiF–NaF–BeF_2$ (15–58–27 mol%) and $LiF–NaF–BeF_2$ (17–58–25 mol%)) and in both cases found good agreement with the experimental data, which gave legitimacy to their approach.

Assuming that the density of the recommended fuel matrix ($LiF–NaF–BeF_2$ (20.6–57.9–21.5 mol%)) follows eqn [13], we can estimate the density of the fuel with the contribution of 1.3 mol% PuF_3, using the additive law of molar volumes. For this calculation, we need to know the molar volume of pure liquid PuF_3, which, to our best knowledge, has not been determined experimentally. To derive this quantity, we assume that liquid PuF_3 has the same molar volume as CeF_3, which was obtained from the density measured by Kirshenbaum and Cahill[67] for the temperature range of 1700–2200 K. For its similar chemical behavior, CeF_3 is considered as a proxy compound to the plutonium species, a consideration that is supported by the comparison of the ionic radii of Ce^{3+} and Pu^{3+}, which are nearly identical, 115 pm for Ce^{3+} and 114 pm for Pu^{3+}. The density function of pure liquid PuF_3 thus obtained is:

$$\rho(\mathrm{kg\,m^{-3}}) = 9550.6 - 1.4296T(\mathrm{K}) \qquad [14]$$

giving

$$\rho(\mathrm{kg\,m^{-3}}) = 2759.9 - 0.5730T(\mathrm{K}) \qquad [15]$$

for the fuel composition ($LiF–NaF–BeF_2–PuF_3$ (20.3–57.2–21.2–1.3)).

To estimate viscosity, Khokhlov *et al.*[65] applied a similar approach as in the case of density. According to their report, the input data were the experimental results of the molar viscosities of binary $LiF–BeF_2$, $NaF–BeF_2$,[56] and LiF–NaF melts.[68] The obtained temperature function of kinematic viscosity of the $LiF–NaF–BeF_2$ (22–56.7–21.3 mol%) composition is shown in **Figure 16**. The same figure shows a comparison of the estimated curve with the experimental data measured by Ignatiev *et al.*[69,70] and there is a close agreement between both sets of results. The corresponding dynamic viscosity of the $LiF–NaF–BeF_2$ (22–56.7–21.3 mol%) composition is given in the following equation:

$$\log_{10}\eta(\mathrm{mPa\,s}) = -1.0018 + (1617.4/T(\mathrm{K})) \qquad [16]$$

As this composition is very close to the recommended fuel choice, neglecting the influence of addition of a relatively small amount of PuF_3 (1.3 mol%), we recommend eqn [16] as a viscosity function of the $LiF–NaF–BeF_2–PuF_3$ (20.3–57.1–21.2–1.3 mol%) fuel.

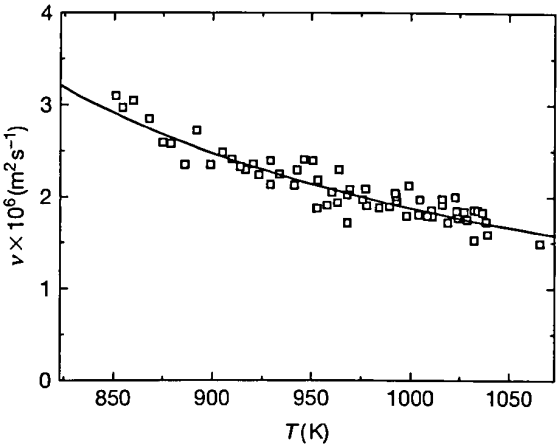

Figure 16 Kinematic viscosity of the $LiF–NaF–BeF_2$ (22–56.7–21.3 mol%) melt: (—) estimated data from Khokhlov *et al.*[65]; (□) experimental data by Ignatiev *et al.*[69,70] Reproduced from Beneš, O.; Konings, R. J. M. *J. Fluor. Chem.* **2009**, *130*, 22–29.

3.13.4.4.5 NaF–$NaBF_4$

The density of $NaF–NaBF_4$ (8–92 mol%) was measured by Cantor[53] from 673 to 864 K. The results can be represented by the equation:

$$\rho(\mathrm{kg\,m^{-3}}) = 2446.3 - 0.711T(\mathrm{K}) \qquad [17]$$

The viscosity of $NaF–NaBF_4$ (8–92 mol%) was measured by Cantor[53] from 682 to 810 K. The results can be represented by the equation:

$$\eta(\mathrm{mPa\,s}) = 0.0877\exp(2240/T(\mathrm{K})) \qquad [18]$$

3.13.4.4.6 LiF–NaF–KF

The density of the eutectic melt of the LiF–NaF–KF system has been measured by Chrenková *et al.*[71] for the temperature range of 940–1170 K. The exact composition of the LiF–NaF–KF melt measured in their study was $x(\mathrm{LiF}) = 0.465$, $x(\mathrm{NaF}) = 0.115$, and $x(\mathrm{KF}) = 0.420$, thus corresponding to the eutectic composition found by Bergmann and Dergunov.[45] The density as a function of temperature of the eutectic composition has also been reported by Powers *et al.*[64] for an unspecified temperature range. As shown in **Figure 17**, the data by Chrenková *et al.* and Powers *et al.* differ significantly. The results of Chrenková *et al.* are close to the density that is calculated assuming ideal behavior and the curve has almost the same

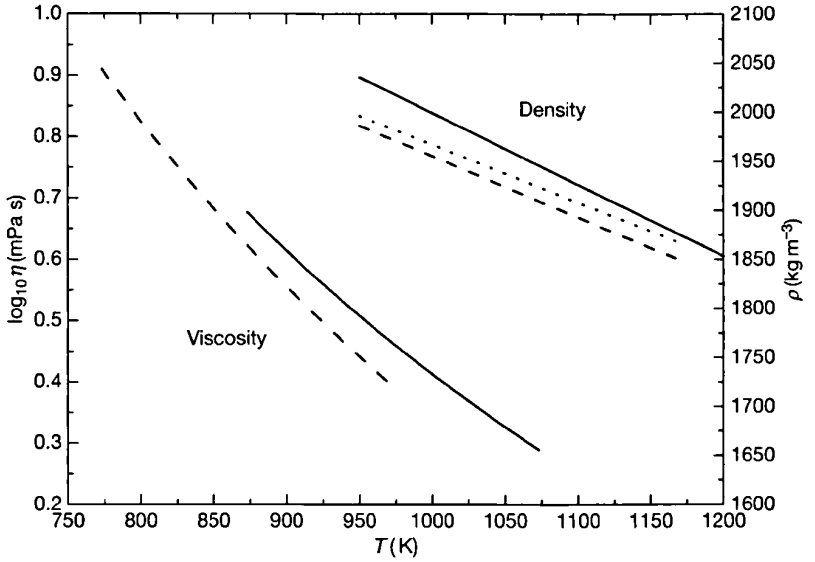

Figure 17 Viscosity and density functions of temperature reported by Chrenková *et al.*[71] (– – –) and Powers *et al.*[64] (——). For comparison, the ideal density behavior is represented by a dotted line. Reproduced from Beneš, O.; Konings, R. J. M. *J. Fluor. Chem.* **2009**, *130*, 22–29.

slope, which is consistent with our observations that most of these fluoride systems are ideal. For this reason, we recommend the data by Chrenková *et al.*:

$$\rho(\text{kg m}^{-3}) = 2579.3 - 0.6240T(\text{K}) \quad [19]$$

The viscosity of the eutectic melt of the LiF–NaF–KF system has been measured by Chrenková *et al.*[71] for the temperature range of 773–973 K and Powers *et al.*[64] for the temperature range of 873–1073 K. The comparison between the data by Chrenková *et al.* and by Powers *et al.* is shown in **Figure 17**. The data by Chrenková *et al.* have been selected:

$$\log_{10}\eta(\text{mPa s}) = -1.6044 + 1944/T(\text{K}) \quad [20]$$

3.13.4.5 Heat Capacity and Thermal Conductivity

3.13.4.5.1 LiF–BeF_2

The heat capacity of liquid LiF–BeF_2 (66–34 mol%) has been measured by Hoffman and Cooke (as cited in Cantor *et al.*[72]), and Douglas and Payne,[73] who obtained 2.41 J K^{-1} g^{-1} (unknown temperature range) and 2.37 J K^{-1} g^{-1} (773–873 K), respectively. The value C_p(LiF–BeF_2 (66–34 mol%)) = 2.39 J K^{-1} g^{-1} has been selected.

The thermal conductivity of LiF–BeF_2 (66–34 mol%) has been measured by Cooke (as reported in Cantor *et al.*[72]) to be 1.0 W m^{-1} K^{-1}, independent of the temperature. Some time later, Cooke *et al.*[74] reported more detailed results, indicating that the thermal conductivity increases slightly, from $\lambda = 1.0$ W m^{-1} K^{-1} at 923 K, to about 1.2 W m^{-1} K^{-1} between 1023 and 1133 K. Kato *et al.*[75] measured the thermal diffusivity of the compositions 66–34 mol% and 53–47 mol%. From their results, we calculate 1.1 W m^{-1} K^{-1} for the 66–34 mol% composition, which is in good agreement with Cooke's results, and we recommend λ (LiF–BeF_2 (66–34)) = 1.1 W m^{-1} K^{-1}.

3.13.4.5.2 LiF–AnF_4

To our best knowledge, heat capacity or thermal conductivity have not been measured for the LiF–ThF_4 system. We have estimated the heat capacity of the LiF–ThF_4 (78–22 mol%) composition on the basis of the comparison between the ideal heat capacity and the measured data from other fluoride systems taken from Powers *et al.*[64] The average positive deviation from the ideal behavior has been found to be 11%. If we combine this difference with the ideal heat capacity of the LiF–ThF_4 (78–22 mol%) composition, we obtain our suggested value: $C_p = 1.0$ J g^{-1} K^{-1}.

There are not enough data to accurately estimate the thermal conductivity of the LiF–ThF_4 (78–22 mol%) composition; however, we suggest that the value be slightly higher than the value of the LiF–BeF_2 (66–34 mol%) composition and close to

the value for LiF–BeF_2–ThF_4 (71.7–16–12.3 mol%) composition, which was derived for $T = 1023$ K (see **Section 3.13.4.5.3**). Our suggested value for LiF–ThF_4 (78–22 mol%) composition is $\lambda = \sim 1.5\ W\ m^{-1}\ K^{-1}$.

3.13.4.5.3 LiF–BeF_2–ThF_4

Araki and Kato[76] measured the thermal diffusivity of liquid LiF–BeF_2–ThF_4 (64–18–18 mol%), from which they derived the thermal conductivity using their heat capacity data and an estimated density. The results indicate an almost constant value in the temperature range of 850–1000 K: 0.95–0.98 $W\ m^{-1}\ K^{-1}$. The recommended heat capacity according to Araki and Kato is $C_p = 1.23\ J\ g^{-1}\ K^{-1}$. Both data, heat capacity and thermal conductivity, are measured for a LiF–BeF_2–ThF_4 composition that is slightly different from the one considered in this work (71.7–16.0–12.3 mol%). Cooke *et al.*[74] reported (in graphical form only) the thermal conductivity of liquid LiF–BeF_2–ThF_4–UF_4 (67.5–20–12–0.5 mol%) for the temperature range of 800–1150 K. The data scatter around $\lambda = 1.2$–$1.4\ W\ m^{-1}\ K^{-1}$, with a suggested maximum at 973 K. This result is somewhat different from that of Araki and Kato.[76] As the results for liquid LiF–BeF_2 from both groups are in good agreement, the variation probably arises from differences in BeF_2 and MF_4 content (where M = Th, U, and Zr). The results from the above-mentioned sources[74,76] indicate that in the measured composition range, the thermal conductivity decreases with increasing ($BeF_2 + MF_4$) content as indicated in **Figure 18**. The LiF–BeF_2–ThF_4 (71.7–16.0–12.3 mol%) composition is just outside this range ($x(BeF_2 + MF_4) = 28.3$ mol%), and linear extrapolation would suggest $\lambda = 1.51\ W\ m^{-1}\ K^{-1}$ at $T = 1023$ K (solid line in **Figure 18**). However, such linear extrapolation would suggest a relatively high thermal conductivity of LiF–ThF_4 (78–22 mol%). Alternatively, one could extrapolate the results in a nonlinear way (dashed line in **Figure 18**). This would suggest $\lambda = 1.49\ W\ m^{-1}\ K^{-1}$ at $T = 1023$ K, which is very close to previously established value. In this case, the thermal conductivity of LiF–ThF_4 (78–22 mol%) is $1.6\ W\ m^{-1}\ K^{-1}$, which is more realistic. For LiF–BeF_2–ThF_4 (71.7–16.0–12.3) composition we recommend:

$$\lambda = 1.5\ W m^{-1}\ K^{-1} \qquad [21]$$

The heat capacity of the quaternary LiF–BeF_2–ThF_4–UF_4 (71–16–12–1 mol%) composition, which is nearly identical to our reference selection (LiF–BeF_2–ThF_4 (71.7–16–12.3 mol%)), has been reported in Briant and Weinberg,[63] giving $C_p = 1550\ J\ kg^{-1}\ K^{-1}$. This value is also fairly close to the estimated value, based on the approach published by Khokhlov *et al.*[65] (discussed in the following section), which gives $C_p = 1.506\ J\ g^{-1}\ K^{-1}$. We select the measured value, $C_p = 1.550\ J\ g^{-1}\ K^{-1}$.

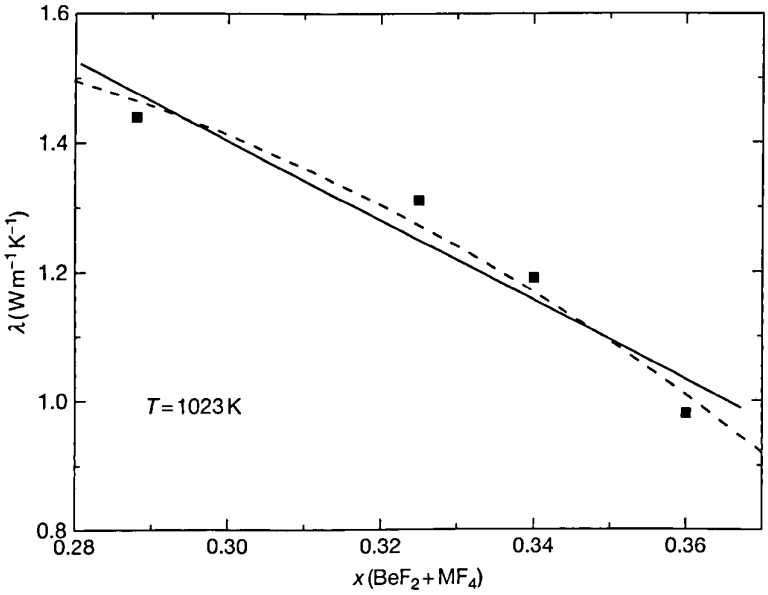

Figure 18 Extrapolation of the thermal conductivity of the LiF–BeF_2–ThF_4 (71.7–16.0–12.3 mol%) composition at $T = 1023$ K. (—) linear fit; (– – –) polynomial fit. (■) Experimental data from Cooke *et al.*[74] and Araki and Kato.[76] Reproduced from Beneš, O.; Konings, R. J. M. *J. Fluor. Chem.* **2009**, *130*, 22–29.

3.13.4.5.4 LiF–NaF–BeF_2–PuF_3

Because of the lack of experimental data on the heat capacity of the actinide-containing salts, it is difficult to properly assess the value for the LiF–NaF–BeF_2–PuF_3 (20.3–57.1–21.2–1.3 mol%) composition. However, Khokhlov *et al.*[65] recently evaluated the heat capacity of more than 30 fluoride salts and found a simple empirical dependence on the inverse molar mass (1/M) by the following equation:

$$C_p(\mathrm{J\,K^{-1}g^{-1}}) = 0.2916 + 0.00802 \times 10^4/\mathrm{M} \quad [22]$$

Using the above equation, the heat capacity for the fuel composition from **Table 3** is calculated as 2.15 $\mathrm{J\,K^{-1}\,g^{-1}}$. This value is fairly close to the experimentally determined heat capacity of the plutonium-free LiF–NaF–BeF_2 (24–53–23 mol%) composition, which was found at 2.26 $\mathrm{J\,K^{-1}\,g^{-1}}$. Because this composition is similar to the fuel composition and its heat capacity is only slightly higher than that found for the fuel composition using eqn [22], we recommend 2.15 $\mathrm{J\,K^{-1}\,g^{-1}}$ as a reasonable estimate of the heat capacity.

Because of the lack of experimental data, it is difficult to assess the thermal conductivity of the complicated salt mixtures, such as plutonium-containing fuel; however, Khokhlov *et al.*[65] analyzed the experimental values of the thermal conductivity determined earlier for molten chlorides, bromides, and iodides of alkali metals and their mixtures and deduced an equation describing the experimental results within the measurement errors. The obtained equation depends only on temperature T (expressed in K) and the molar weight M of the salt mixture (expressed in g $\mathrm{mol^{-1}}$) and is given by:

$$\lambda(\mathrm{W\,m^{-1}K^{-1}}) = -0.34 + 0.5 \times 10^{-3}T + 32.0/\mathrm{M} \quad [23]$$

Using this equation, the thermal conductivity of the LiF–NaF–BeF_2–PuF_3 (20.3–57.1–21.2–1.3) composition gives the following function of temperature:

$$\lambda(\mathrm{W\,m^{-1}K^{-1}}) = 0.402 + 0.5 \times 10^{-3}T \quad [24]$$

3.13.4.5.5 NaF–$NaBF_4$

The heat capacity of the NaF–$NaBF_4$ (8–92 mol%) melt has been determined by Dworkin (as mentioned in Cantor[53]) as $C_p = 1.506\,\mathrm{J\,g^{-1}\,K^{-1}}$.

The thermal conductivity of the NaF–$NaBF_4$ (8–92 mol%) melt has been reported by Cooke *et al.*[74] for the temperature range of 740–1000 K. However, they have reported their results only in a graphical form without listing the exact values or equations. Thus, their data have been obtained by digital subtraction from the figure, and the temperature function of the thermal conductivity has been determined by a linear fit, giving:

$$\lambda(\mathrm{W\,m^{-1}K^{-1}}) = 0.66 - 2.37 \times 10^{-4}T(\mathrm{K}) \quad [25]$$

It is interesting to compare these results with those of Cantor *et al.*,[72] who reported preliminary measurements of the thermal conductivity of pure liquid $NaBF_4$, finding $\lambda = 0.51\,\mathrm{W\,m^{-1}\,K^{-1}}$, which is, on average, slightly higher than that of the NaF–$NaBF_4$ (8–92 mol%) eutectic composition.

3.13.4.5.6 LiF–NaF–KF

Powers *et al.*[64] reported the heat capacity of the LiF–NaF–KF (46.5–11.5–42 mol%) melt measured at $T = 973$ K, giving $C_p = 1.88\,\mathrm{J\,g^{-1}\,K^{-1}}$. This value is significantly higher than that obtained from the ideal behavior ($C_{p,\,\mathrm{ideal}} = 1.66\,\mathrm{J\,g^{-1}\,K^{-1}}$).

The same authors measured the thermal conductivity of the eutectic composition, giving $\lambda = 4.5$ $\mathrm{W\,m^{-1}\,K^{-1}}$. This value is much higher than the measurement (773–1173 K) by Ewing *et al.*, $\lambda = 0.6$ $\mathrm{W\,m^{-1}\,K^{-1}}$. Smirnov *et al.*[77] measured the thermal conductivity of eutectic LiF–NaF–KF (46.5–11.5–42 mol%) from 790 to 1080 K and obtained $\lambda = 0.36 + 5.6 \times 10^{-4}T(\mathrm{K})\,\mathrm{W\,m^{-1}\,K^{-1}}$, giving 0.8 $\mathrm{W\,m^{-1}\,K^{-1}}$ at $T = 773$ K. Kato *et al.*[75] measured the thermal diffusivity of LiF–NaF–KF (46.5–11.5–42 mol%) in the temperature range of 730–823 K and obtained $a = 7.6 \times 10^{-4} + 6.3 \times 10^{-7}T(\mathrm{K})\,\mathrm{m^2\,h^{-1}}$, which yields 0.8 $\mathrm{W\,m^{-1}\,K^{-1}}$ at $T = 773$ K when combined with the selected heat capacity and density values. We thus recommend:

$$\lambda(\mathrm{W\,m^{-1}K^{-1}}) = 0.36 + 5.6 \times 10^{-4}T(\mathrm{K}) \quad [26]$$

3.13.4.6 Vapor Pressure

3.13.4.6.1 LiF–BeF_2

According to the thermodynamic data taken from Beneš and Konings,[25] the vapor pressure of the LiF–BeF_2 (66–34 mol%) composition has been calculated for the temperature range between 823 and 1473 K, which covers the typical operating temperature range of the MSR and also describes the vapor pressure at high temperature in order to simulate the fuel behavior during accidental conditions. The result is given in the equation below:

$$\log_{10} p(\mathrm{Pa}) = 11.914 - 13\,003/T(\mathrm{K}) \quad [27]$$

3.13.4.6.2 LiF–AnF_4

According to the thermodynamic data obtained from van der Meer *et al.*,[36] the vapor pressure of the

$LiF–ThF_4$ (78–22 mol%) composition has been calculated for the temperature range between 839 and 1473 K. The result is given in the equation below:

$$\log_{10} p(\text{Pa}) = 11.902 - 12\,989/T(\text{K}) \quad [28]$$

The vapor pressure of the $LiF–ThF_4–UF_4$ (78–18–4 mol%) composition is slightly lower compared to a system with no UF_4 content. The calculated boiling temperature of the $LiF–ThF_4$ (78–22 mol%) composition is $T = 1874$ K.

3.13.4.6.3 $LiF–BeF_2–ThF_4$

According to the thermodynamic data by van der Meer *et al.*,[36] the vapor pressure of the $LiF–BeF_2–ThF_4$ (71.7–16.0–12.3 mol%) composition has been calculated for the temperature range of 823–1473 K and the obtained result is shown in the following equation:

$$\log_{10} p(\text{Pa}) = 11.158 - 10\,790.5/T(\text{K}) \quad [29]$$

The calculated boiling temperature of the $LiF–BeF_2–ThF_4$ (71.7–16.0–12.3 mol%) composition is $T = 1744$ K.

3.13.4.6.4 $LiF–NaF–BeF_2–AnF_3$

In the study by Beneš and Konings,[25] the vapor pressure of the potential fuel composition ($LiF–NaF–BeF_2–PuF_3$ (20.3–57.1–21.2–1.3 mol%)) has been calculated, and the results are reported in Figure 19, where the total vapor pressure is highlighted by a bold curve, whereas the most volatile species are reported by thin lines. The graph does not include Pu containing species because even the most volatile among these, PuF_4, has a much lower pressure than the species reported, and therefore they have been excluded from the figure. The total vapor pressure is represented by the following equation:

$$\log_{10} p(\text{Pa}) = 11.6509 - 12\,827/T(\text{K}) \quad [30]$$

which gives $p = 0.001$ Pa and $p = 0.046$ Pa at the designed inlet temperature ($T_{\text{inlet}} = 873$ K) and the outlet temperature ($T_{\text{outlet}} = 988$ K) of the MOSART reactor,[6] respectively. Both values are very low, and hence the composition shift of the fuel as a consequence of the incongruent vaporization can be neglected. The calculated boiling temperature is $T = 1973$ K.

3.13.4.6.5 $NaF–NaBF_4$

The vapor pressure of BF_3 in the $NaF–NaBF_4$ system has been measured by Cantor *et al.*[78] They measured the equilibrium of the BF_3 gaseous species over the melt for the composition range of 5–100 mol% $NaBF_4$ and the temperature range of 698–1473 K. However, in their report they 'only' show the results for 900, 1000, and 1100 K. Based on this triplet of data, the vapor pressure equation of $NaF–NaBF_4$ (8–92 mol%) has been determined, giving:

$$\log_{10} p(\text{Pa}) = 11.638 - 6550.6/T(\text{K}) \quad [31]$$

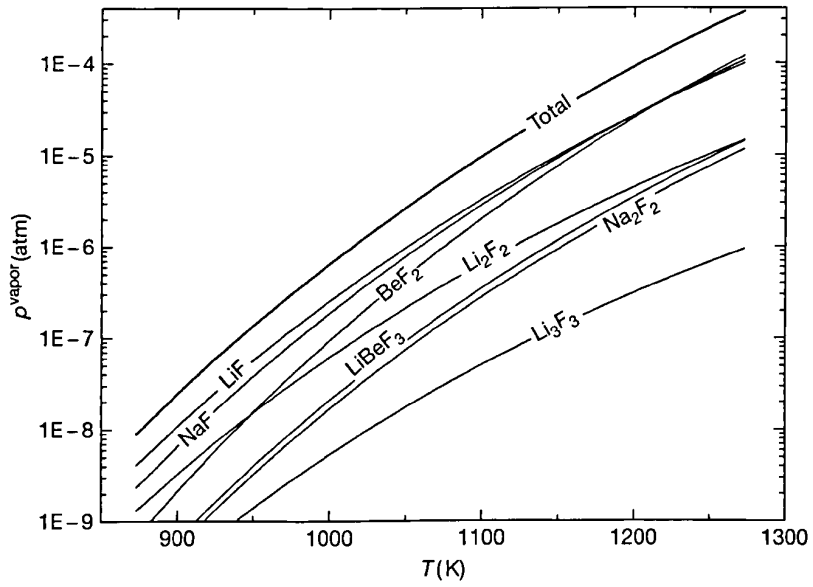

Figure 19 Calculated vapor pressure of the $x(LiF) = 0.203$, $x(NaF) = 0.571$, $x(BeF_2) = 0.212$, $x(PuF_3) = 0.013$ potential fuel composition. Reproduced from Beneš, O.; Konings, R. J. M. *J. Chem. Thermodyn.* **2009**, *41*, 1086–1095.

3.13.4.6.6 LiF–NaF–KF

The vapor pressure of the LiF–NaF–KF (46.5–11.5–42 mol%) composition has been calculated for the temperature range between 823 and 1473 K in a study by Beneš and Konings,[79] on the basis of the thermodynamic data taken from Beneš and Konings.[48] The result is given by the equation below:

$$\log_{10} p(\text{Pa}) = 10.748 - 10\,789/T(\text{K}) \quad [32]$$

3.13.5 Role of Oxygen Impurities

In the previous section, the physicochemical properties of pure fluoride salts have been discussed. However, the behavior of these systems can be significantly affected by the presence of the oxide ion that might be resulting from contamination of the salt system; for example, the presence of reactive oxides such as H_2O can result in precipitation of the UO_2 phase.[80] Therefore, the effect of added oxide on the fuel mixture containing LiF, BeF_2, ThF_4, UF_4, and PaF_4 has been investigated in several studies,[81–88] as reported in Rosenthal *et al.*[80] who give a summary of the main conclusions from these works is given. It has been found that the solubility of the actinide dioxides in the MSBR fuel salt is low and it decreases in the order, ThO_2, PaO_2, UO_2, and PuO_2. The temperature functions of the solubilities of these oxides were estimated in the same study as follows:

$$\log_{10} Q_{ThO_2} = -2.86 - 3280/T(\text{K}) \quad [33]$$

$$\log_{10} Q_{PaO_2} = -2.86 - 4920/T(\text{K}) \quad [34]$$

$$\log_{10} Q_{UO_2} = -2.86 - 5660/T(\text{K}) \quad [35]$$

$$\log_{10} Q_{PuO_2} = -2.86 - 7100/T(\text{K}) \quad [36]$$

where

$$Q_{MO_2} = x_{M^{4+}} x_{O^{2-}}^2 \quad [37]$$

The ThF_4 concentration in the MSBR concept is equal to $x = 0.12$, and it has been shown[80] that at such concentrations of thorium, the ThO_2 precipitation at $T = 773$ K will start for $x_{O^{2-}} \geq 8 \times 10^{-4}$.

Protactinium is produced in thorium-containing breeder fuel by neutron capture, and both tetravalent and pentavalent species of protactinium are stable. Thus, in addition to PaO_2, Pa_2O_5 can precipitate in the oxide form. As reported in Rosenthal *et al.*,[80] this oxide is very insoluble in the fluoride mixture of the MSBR composition given by:

$$\log_{10} Q_{Pa_2O_5} = 0.91 - 12\,760/T(\text{K}) \quad [38]$$

where

$$Q_{Pa_2O_5} = x_{Pa^{5+}} x_{O^{2-}}^{5/2} \quad [39]$$

Whether Pa_2O_5 will precipitate or not depends on three factors: oxide and protactinium concentrations, and the oxidation state of the fuel, which, in the MSR, is controlled by the UF_4/UF_3 ratio, as discussed in **Section 3.13.8**. As reported in Rosenthal *et al.*,[80] with 100 ppm Pa and 30 ppm oxide present, the UF_4/UF_3 ratio must be at least 10^5 in order to start the Pa_2O_5 precipitation. Nevertheless, such oxidizing conditions are easily avoided, as the typical UF_4/UF_3 ratio in the MSR is set to 100 (see **Section 3.13.8**).

Even stronger oxidizing conditions ($UF_4/UF_3 > 10^8$) are required to precipitate PuO_2, and hence this species is avoided in the MSR fuel as well.

Although the Pa_2O_5 and PuO_2 species will not be formed in the fuel salt, the other actinide dioxides UO_2, ThO_2, and PaO_2 can be formed under the redox conditions of the MSR and, due to the very low solubilities of these species in the fluoride matrix (as given by eqns [33]–[36]), they can easily precipitate in the solid form. Therefore, it is important to keep the fuel salt free from any oxide contamination to avoid this inadvertent event. This will certainly require some care but, as mentioned in Rosenthal *et al.*,[80] the results of the MSRE project have shown that the oxide content can be maintained at an adequately low level in order to achieve successful long-term operation of the MSR.

3.13.6 Electroanalytical Chemistry

Surprisingly, very little experimental work has been done on the electrochemical properties of the main ions in molten fluoride salts. For the LiF–BeF_2 system, some direct measurements of the standard potentials have been made. The standard potentials of the main ions in the liquid LiF–BeF_2 (67–33) melt have been reported by Baes.[89–91] He has made an extensive analysis of the available literature, which is essentially based on a comparative scale as only the Be^{2+}/Be^0 couple has been measured electrochemically[92]:

$$\text{Be(cr)} + 2\text{HF(g)} = \text{BeF}_2\text{(sln)} + \text{H}_2\text{(g)} \quad [\text{I}]$$

Using equilibrium constants, Gibbs energies of the solutes, and activity coefficients, Baes derived the

Table 6 Standard potential in LiF–BeF_2 (66–34) relative to the HF(g)/H_2 couple, $E/V = a + bT$ (K)

Cell reaction	*a*	*b* × 10^3
$Li^+(sln) + e^- = Li(cr)$	−3.322	0.763
$Be^{2+}(sln) + 2e^- = Be(cr)$	−2.460	0.694
$1/2F_2(g) + e^- = F^-(sln)$	+2.827	0.044
$Th^{4+}(sln) + 4e^- = Th(cr)$	−2.498	0.720
$U^{3+}(sln) + 3e^- = U(cr)$	−2.059	0.626
$U^{4+}(sln) + 4e^- = U(cr)$	−1.851	0.807
$UF_6(g) + 2e^- = U^{4+}(sln) + 6F^-(sln)$	−1.439	0.200
$Pu^{3+}(sln) + 3e^- = Pu(cr)$	−2.313	0.788
$Cr^{2+}(sln) + 2e^- = Cr(cr)$	−0.898	0.508
$Fe^{2+}(sln) + 2e^- = Fe(cr)$	−0.527	0.516
$Ni^{2+}(sln) + 2e^- = Ni(cr)$	−0.357	0.830

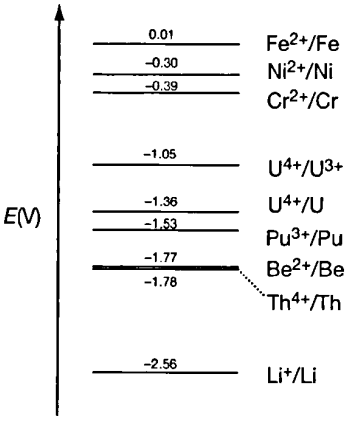

Figure 20 Standard potential in LiF–BeF_2 (66–34) relative to the HF(g)/H_2 couple calculated at $T = 1000$ K.

values as a function of temperature as given in Table 6, which gives the standard potentials for the main salt carrier elements, the actinides, and some elements of structural materials. Figure 20 shows the electrochemical potentials calculated for $T = 1000$ K.

In a recent study, Chamelot *et al.*[93] studied the electrochemical potentials of ThF_4, NdF_3, and GdF_3 in the LiF–CaF_2 (77–23) solvent in order to demonstrate the reprocessing scheme of the molten salt fuel. The LiF–CaF_2 system has been selected in their study as it has a lower melting point compared to pure LiF. The experimental results are given in Table 7 and show that the LiF–CaF_2 (77–23) solvent can be alternatively used to reduce Th, Nd, and Gd from this salt as the redox potentials of $M^{x+} + xe^- \rightarrow M^0$ (M = Th, Nd, Gd) reactions are more positive than in the case of the $Li^+ + e^- \rightarrow Li^0$ reaction and so are reduced prior to the solvent. These authors also concluded that the LiF–BeF_2 (67–33) composition, as the typical MSR carrying

Table 7 Standard potential in LiF–CaF_2 (77–23) relative to the F_2/F^- pair measured by Chamelot *et al.*[93] at $T = 1100$ K

Cell reaction	E^0/V
$Li^+(sln) + 1e^- = Li(cr)$	−5.33
$Th^{4+}(sln) + 4e^- = Th(cr)$	−4.57
$Nd^{3+}(sln) + 3e^- = Nd(cr)$	−4.88
$Gd^{3+}(sln) + 3e^- = Gd(cr)$	−4.93

Table 8 Standard potential in LiF–CaF_2 (77–23) relative to the F_2/F^- pair measured by Hammel *et al.*[94] at $T = 993$ K

Cell reaction	E^0/V
$Li^+(sln) + 1e^- = Li(cr)$	−5.44
$U^{3+}(sln) + 3e^- = U(cr)$	−4.53
$U^{4+}(sln) + 1e^- = U^{3+}(sln)$	−3.81

salt, has a much narrower electrochemical window and is not suitable for the reduction of the Th, Nd, and Gd metals.

Hammel *et al.*[94] measured the electrochemical potential of UF_4 in LiF–CaF_2 (77–23) and found UF_4 less stable than the solvent components and thus suitable for reduction from this salt. The values of the redox potentials obtained in their study are summarized in Table 8, showing the value for the $Li^+ + e^- \rightarrow Li^0$ reaction in fair agreement with the work of Chamelot *et al.*[93]

3.13.7 Radiation Stability of Molten Salts

As in ceramic fuels, the fuel carrier in a MSR will be subjected to various types of radiation that can cause damage, such as α- and β-decay, γ-radiation, and neutron and fission products. But unlike ceramic fuels, a liquid does not have a lattice structure (long-range order) that can be distorted.

As reported by Blankenship,[95] radiolytic formation of F_2 occurs in the fluoride salts at low temperatures ($T < 100$ °C), but, because all the salts considered as MSR fuel are in the solid state at these temperatures, the evolution rate is somehow limited by a slow fluorine diffusion within the crystal. At higher temperatures, a reverse reaction counteracts primary radiolysis events, which happens for most of the salts far below their melting points. It has been demonstrated that, during this recombination process, F_2 reacts more rapidly with salts that have primarily lost their fluorine atoms and, thus, the

F_2 buildup in the reactor is eliminated.[95] Because the MSR operates at high temperatures, the recovery process is rapid and radiation damage to the salt is very small. This has been confirmed in separate experiments, using accelerators, and in in-pile tests for the ARE and MSRE projects. None of these experiments have revealed indications that the fluoride salts are unstable in radiation fields.[8,95] It is believed that this radiation stability is responsible for the demand that only very stable salts must be considered in the reactor in order to keep the construction alloys thermodynamically stable with respect to the salt.

3.13.8 Fission Product Behavior

The fission products that are formed during the operation of the MSR can be divided into three main groups based on their solubilities in the carrying matrix: noble gases, stable salt-soluble fluorides, and noble metals that are very difficult to dissolve in the fluoride matrix. Whether the fission product will or will not be dissolved by the salt is determined by the redox potential of the salt. As demonstrated in the MSRE project, the redox potential of the salt is controlled by the UF_4/UF_3 ratio in such way that the corrosion of the structural material, for example, leaching of chromium (the least stable element in the Ni-based alloys, see **Section 3.13.9**) from the Hastelloy-N,[83] is inhibited. As reported by Rosenthal *et al.*,[80] the UF_4/UF_3 ratio in the MSRE was ~100. It is shown in **Figure 21** that at this concentration the ratio of dissolved chromium in the form of CrF_2 and its metal form is $<10^{-5}$. Taking into account that the UF_4/UF_3 ratio is set in such way not to form chromium fluoride, one can assume that fluorides that have more negative free energy of formation ΔG_f^0 according to the general reaction:

$$x\mathrm{M}_{\mathrm{metal}} + y\mathrm{F}_{2\mathrm{gas}} \rightarrow x\mathrm{MF}_{2y} \quad \Delta G_f^0 \qquad [\mathrm{II}]$$

will dissolve in the fuel, whereas the ones that have higher ΔG_f^0 of the above given reaction will precipitate in the form of insoluble metals.

During the operation of the MSR, free fluorine is formed from the fission processes. This fluorine preferably reacts with UF_3, increasing the UF_4/UF_3 ratio and thus changing the redox potential of the salt. This will certainly increase the corrosion rate of the structural material; therefore, the UF_3 concentration must be readjusted. This is achieved by adding small amounts of pure metals, for example, beryllium, which absorb fluorine. In the MSRE, a beryllium rod was kept immersed in the salt until the UF_3 concentration reached the correct value. On the other hand, as discussed in **Section 3.13.9**, too high

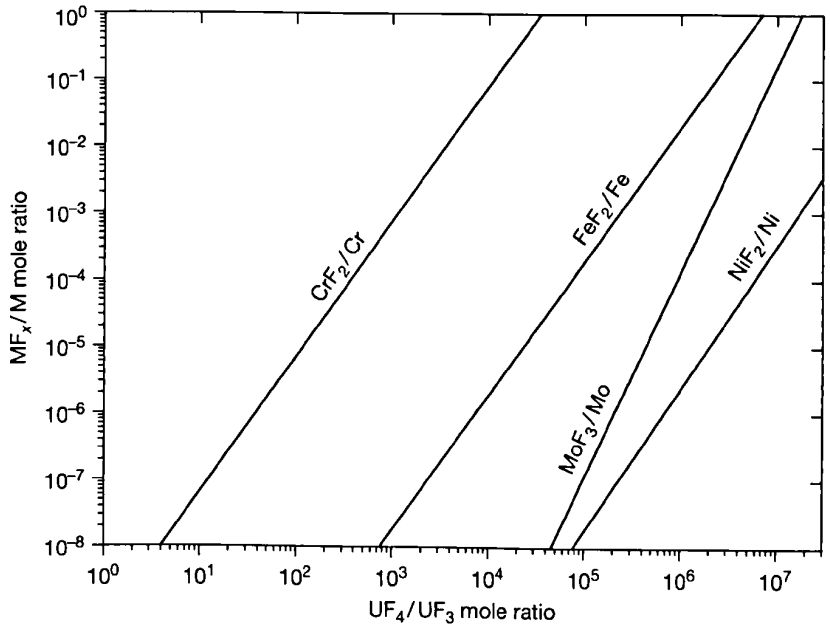

Figure 21 Variation of equilibrium concentration of structural metal fluorides as a function of the UF_4/UF_3 ratio in a molten salt reactor fuel. Reproduced from Rosenthal, M. W.; Haubenreich, P. N.; Briggs, R. B. Tech. Rep. ORNL-4812; 1972.

a content of UF_3 is not allowed in the MSR as it can corrode graphite or other structural components. Hence, one must be able to control the redox potential of the salt in the other direction also to achieve more oxidizing conditions, and thus increasing the UF_4/UF_3 ratio. In the MSRE, this was done by adding NiF_2 into the fuel. At the redox conditions of the MSR, NiF_2 decomposes to metallic nickel and fluorine, which then reacts with UF_3 forming more UF_4 (see **Chapter 5.10, Material Performance in Molten Salts**).

3.13.8.1 Noble Gases

The solubility of inert gases in molten fluoride salts has been measured by a limited number of authors. Grimes *et al.*[96] measured the solubility of He, Ne, Ar, and Xe in $NaF–ZrF_4$ (53–47 mol%) and $NaF–ZrF_4–UF_4$ (50–46–4 mol%); Blander *et al.*[97] measured the solubility of He, Ne, and Ar in LiF–NaF–KF eutectic; and Watson *et al.*[98] measured the solubility of He, Ne, Ar, and Xe in $LiF–BeF_2$ (64–36 mol%).

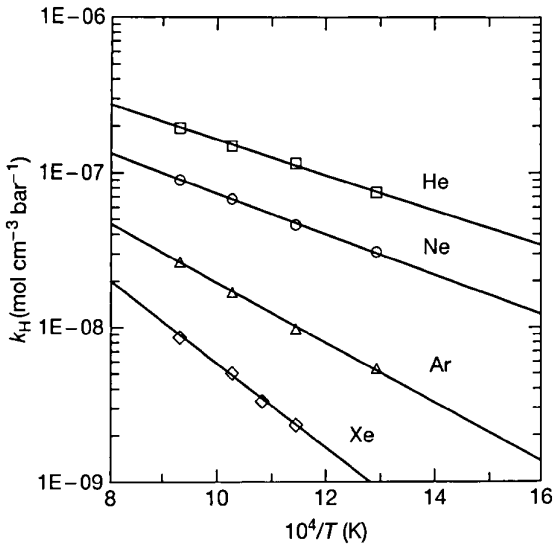

Figure 22 The Henry's constant k_H of noble gases as a function of the reciprocal temperature in molten $LiF–BeF_2$ (64–36). Reproduced from Watson, G. M.; Evans, R. B.; Grimes, W. R.; Smith, N. V. *J. Chem. Eng. Data* **1962**, *7*, 285–287.

These studies all show that the solubilities increase linearly with gas pressure and temperature and decrease with increasing atomic weight of the gas atom. All experimental data confirm that the solubility of these noble gases follows Henry's Law, which says that in very dilute solutions, the pressure is proportional to the mole fraction:

$$p_i = k_H x_i \qquad [40]$$

The proportionality factors k_H derived from the experiments for $LiF–BeF_2$ (64–36 mol%) are plotted in **Figure 22** as a function of the reciprocal temperature and listed in **Table 9**.

As is obvious from the table and the figure, the noble gases are only slightly soluble in molten salts. They can be removed from the fuel by sparging with helium to an off-gas system. As reported in Engel *et al.*,[99] it was demonstrated during the operation of the MSRE that about 80% of ^{135}Xe, the highest noble gas neutron poison, was removed using this method. It was observed in Rosenthal *et al.*[80] that no compounds are formed with noble metals under the MSR conditions, which prevents the noble metals from being chemically bonded to the fuel salt.

3.13.8.2 Salt-Soluble Fission Products

Alkali metals (mainly Rb, Cs), alkali-earth (mainly Sr, Ba), the lanthanides, and Y with Zr, all form stable fluorides and are soluble in the fuel salt. Hence, they are expected to be found completely dissolved in the fuel, except for the ones that have noble gas precursors with relatively long half-lives and these are removed prior to their decay by the off-gas system. It was demonstrated experimentally

Table 9 The Henry's constant k_H of noble gases in molten $LiF–BeF_2$ (64–36 mol%) as a function of the temperature

T (K)	*Solubility ($\times 10^8$ mol cm^{-3})*			
	He	*Ne*	*Ar*	*Xe*
773	7.49 ± 0.07	3.09 ± 0.09	0.54 ± 0.02	
873	11.55 ± 0.39	4.63 ± 0.01	0.98 ± 0.02	0.233 ± 0.002
923				0.333 ± 0.011
973	14.93 ± 0.42	6.80 ± 0.09	1.69 ± 0.10	0.505 ± 0.020
1073	19.48 ± 0.01	9.01 ± 0.15	2.66 ± 0.06	0.863 ± 0.021

Source: Watson, G. M.; Evans, R. B.; Grimes, W. R.; Smith, N. V. *J. Chem. Eng. Data* **1962**, *7*, 285–287.

that these isotopes with noble gas precursors (^{89}Sr and ^{137}Cs) show ratios to the calculated inventory that are significantly lower than those without, which generally scatter around 1.0.[80] Although an online cleanup will be made for the MSR fuel, some of the fission products from this group will remain dissolved in the salt during the lifetime of the reactor. However, as reported, for example, in the MSR FUJI concept,[4] for a thermal spectrum reactor, the accumulation of these fission products will be relatively small, within the tenths of wt%, mostly represented by Zr and lanthanides, followed by cesium. Such low concentrations will only negligibly affect the fuel properties, as demonstrated in a recent study by Beneš and Konings.[31]

3.13.8.3 Insoluble Fission Products

This group of fission products is mostly represented by noble metals that are more thermodynamically stable to oxidation than chromium in the structural alloy, at the redox conditions maintained in the MSR. Therefore, they are expected to be found in the fuel in the metal form. Noble metals that will accumulate in the MSR in significant amounts are isotopes of Nb, Mo, Tc, Ru, Ag, Sb, and Pd. As confirmed by the MSRE,[9,80,100] selenium and tellurium are also expected to be present in the reactor circuit in metal form; however, as discussed in **Section 3.13.9**, the reduction of tellurium in the salt to telluride can be achieved by increasing the UF_3/UF_4 ratio to about 0.05.[101]

As the noble metals are insoluble in the fluoride salt, it is important to understand the state of these fission products within the fuel circuit. Based on the MSRE samples,[101] some metallic particles were found in the helium sparge gas, some were deposited on the metallic surfaces of the primary circuit, and a smaller fraction was found deposited on the graphite specimens. The aim is to avoid the precipitation of these metallic fission products on the structural materials as the deposited material contributes to the heat generation from its decay even after the reactor shutdown, decreasing the overall safety of the MSR. Furthermore, the deposits on the graphite specimens in the case of thermal reactors absorb neutrons during the operation and lead to lower efficiency of the reactor. One way of avoiding this detrimental precipitation is to remove the insoluble fission products by helium bubbling before they interact with the structural materials.

3.13.8.4 Iodine

A separate section is devoted here to iodine, as it does not fit into either of the above-mentioned categories.

At the redox conditions of the MSR, iodine is kept dissolved in the fuel salt in the form of the I^- anion. From the thermodynamic point of view, it would be necessary to have a UF_4/UF_3 ratio of at least 10^4 in order to strip 0.1% of I^- as I_2 in the off-gas system.[100] Such conditions are highly oxidizing and are not allowed as the rate of chromium leaching from the Hastelloy-N would be too high. Based on the MSRE observations, the experimentally obtained inventories of iodine found in the fuel salt mostly ranged somewhere between 30% and 60% of the calculated ones. Why such relatively small amounts were observed is not clear, but one of the possible explanations is that the ^{131}Te precursor of iodine with a half-life of 25 min had been stripped from the fuel before it decayed to ^{131}I or deposited on the surfaces of the reactor vessels.[100]

3.13.9 The Effect of Corrosion Reactions on the Fuel Behavior

Corrosion of the structural materials of the reactor by the molten salt may affect the chemistry and redox conditions of the fuel. The corrosion process to be considered in this context is the oxidation of metals in the alloy phase and their dissolution in the salt phase. From the thermodynamic point of view, Cr is the least stable element in relevant Ni-based alloys such as Hastelloy-N, as can be seen in **Figure 23**. It is not useful to apply a protective coating of, for example, an oxide layer on the structural material for the two following reasons: although some oxides are relatively insoluble in the fluoride melt, most are readily dissolved, and all rapidly recrystallize.[101] Therefore, the clean metal must withstand the corrosive attack of the salt.

As discussed by Briggs,[102] three principal corrosion processes can be distinguished:

- Reactions due to oxides on the metal: Oxide films on the surface of the alloy can be attacked by the fluoride melt:

$$Cr_2O_3 + 3BeF_2(salt) = 2CrF_3(salt) + 3BeO \quad [III]$$

$$FeO + BeF_2(salt) = FeF_2(salt) + BeO \quad [IV]$$

The formed oxides are of little consequence as long as they do not contain fissile elements, but

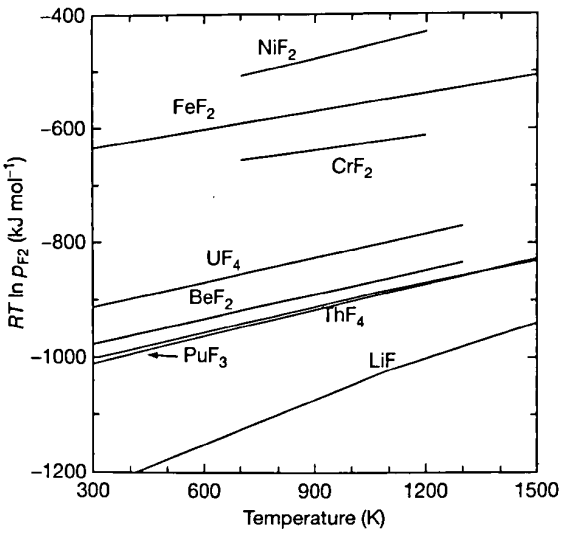

Figure 23 The stability of selected metal fluorides.

the formed fluorides will act as oxidants of Cr in the alloy.

- Reactions with dissolved impurities: In addition to impurities generated by reactions with oxides, impurities may result from incomplete removal of HF or of easily reducible fluorides during the salt purification, which is done by successive reactions with HF–H_2 and H_2. In this case, the following reactions should be considered:

$$\mathrm{Cr(alloy) + 2HF(salt) = CrF_2(salt) + H_2(g)} \quad \text{[V]}$$

$$\mathrm{Cr(alloy) + FeF_2(salt) = CrF_2(salt) + Fe} \quad \text{[VI]}$$

- Reactions with necessary constituents of the melt: The oxidation reaction of alloy components with UF_4 has been suggested to play an important role in the corrosion[103]:

$$\mathrm{Cr(alloy) + 2UF_4(salt) = CrF_2(salt) + 2UF_3(salt)} \quad \text{[VII]}$$

Equation [VII] will define/buffer the electrochemical potential of the salt via the UF_4/UF_3 ratio:

$$K_{47} = \frac{a_{CrF_2}a^2_{UF_3}}{a_{Cr}a^2_{UF_4}} = \frac{(\gamma x)_{CrF_2}(\gamma x)^2_{UF_3}}{(\gamma x)_{Cr}(\gamma x)^2_{UF_4}} \quad [41]$$

where α is the activity and γ is the activity coefficient. Briggs[102] showed that, based on reasonable estimations of the activity coefficients for the above reaction, the equilibrium concentration of CrF_2 is of the order of 130–300 ppm for a fuel with 1% UF_4 contained in Hastelloy-N.

The equilibrium concentration of Cr in the MSRE fuel salt was found to be (72 ± 8) ppm, which after variation of the operation temperature increased to 85 ppm.[104] This is lower than the approximate equilibrium concentration. Also, the observed rates of corrosion in the MSRE have been significantly lower than predicted from thermodynamic data and diffusion theory. It has been postulated that one of the principal reasons for the unexpectedly low values observed is that the metal surfaces of the fuel circuit have been covered with a film of the noble-metal fission products Nb, Mo, Tc, and Ru about 10 Å thick.[104] Such low Cr concentrations in the fuel will not have a large impact on the properties of the fuel salt.

A special paragraph must be devoted to the influence of the fission product tellurium on the corrosion aspects of the fuel salt. When it is present in the metallic form in the fuel, it corrodes Ni-based alloys and embrittles its surface grain boundaries. This embrittlement is a vital issue to consider because, in the long term, it can result in cracking of the structural materials (see **Chapter 5.10, Material Performance in Molten Salts**). As reported in Keiser,[105] an investigation using chromium telluride as tellurium source was carried out in order to understand the mechanism of this type of corrosion. It was concluded that the intergranular embrittlement produced in Hastelloy-N can be significantly reduced by adding 1–2 wt% of niobium into the Hastelloy-N. Another way to suppress the corrosion rate is by increasing the reducing conditions of the fuel, which is done by the increase of the UF_3/UF_4 ratio (done in the MSRE by adding Be metal into the fuel). At such conditions, tellurium would be present as Te^{2-} anion rather than in an 'oxidized' metallic form, and this is less aggressive against the nickel-based alloys. On the other hand, one must be cautious because setting the UF_3/UF_4 ratio too high will result in some parasitic reactions of the UF_3 with graphite (only in case of thermal-moderated reactor) and possibly with other materials within the primary reactor circuit.[101]

3.13.10 Summary and Future Work

The MSR is a very promising concept for the future needs of nuclear energy. It can be designed as a thermal (graphite-moderated) or nonmoderated breeder reactor that produces more fuel from ^{232}Th than it consumes, or as an actinide burner to manage the plutonium and the long-lived minor

actinides (Np, Am, Cm) contained in significant amounts in the nuclear waste coming from current nuclear power plants. For a thermal spectrum reactor, the ideal candidate for the fuel matrix is a mixture of ^{7}LiF and BeF_2 because of its very low neutron capture cross-section; for the nonmoderated spectrum, other fluorides, for example, NaF, can be considered.

A critical review of physicochemical properties of the primary fuel choices of various MSR designs (see **Table 2**) has been done in **Section 3.13.4**. From the evaluated data, we can conclude the following:

- The thermodynamic description of the fuel systems is available and, based on these results, the liquidus temperatures, vapor pressures, and the solubility of actinide fluorides in the fuel solvent can be adequately derived. However, the addition of other matrix components must be investigated in order to decrease the melting temperature of the nonmoderated MSR fuel.
- The density and the derived molar volume of most binary liquid systems can be described in terms of ideal mixtures, which means that the density can be calculated by linear interpolation of the molar volumes of the end members.
- The viscosity of fluoride systems shows significant nonideal mixing behavior. Notably, the binary LiF–ThF_4 system shows a strong positive deviation from ideal behavior over a wide composition range. The same has been found in the LiF–BeF_2 system. Based on these observations, it is not possible to accurately estimate the viscosity of the fluoride salts, and therefore more measurements are required.
- Data on experimental heat capacity of molten fluoride systems containing actinide fluorides are generally lacking. Khokhlov *et al.*[65] derived an estimation equation that is based only on the reverse molar mass of the salt mixture. However, this method must be considered only as an approximation as it sometimes gives relatively large deviations to the experimentally determined heat capacity (e.g., pure LiF or NaF). Thus, more measurements are required in order to describe the heat capacity behavior of the liquid fluoride solutions more precisely.
- Experimental data for the thermal conductivity of molten fluoride systems are generally lacking. Although Khokhlov *et al.*[65] recently derived an estimation method for this quantity on the basis of the available data for the molten chlorides, bromides, and iodides, more measurements are needed in order to justify his approach.

Attention must be also given to the corrosion of the fuel salt against the structural material. It has been reported in **Sections 3.13.8** and **3.13.9** that the corrosion rate in MSRE was maintained at a very low level during the operation of the reactor, mainly by controlling the redox potential of the salt via the UF_4/UF_3 ratio and also by frequent fission product removal; however, the outlet temperature of the MSRE was 927 K, which is rather low for current interests. The demand for a higher temperature regime leads to a higher corrosion rate of the Ni-based alloys (e.g., Hastelloy-N used in the MSRE); hence, new structural materials must be investigated that would withstand the attack of the salt at elevated temperatures.

Acknowledgments

The authors want to acknowledge Dr. V. Ignatiev and Dr. V. Khokhlov for their fruitful discussions on the topic of the molten salt reactor.

References

1. US DOE Nuclear Energy Research Advisory Committee and the Generation IV International Forum, A Technology Roadmap for Generation IV Nuclear Energy Systems, http://www.ne.doe.gov/genIV/documents/gen_iv_roadmap.pdf.
2. Robertson, R. C. Technical Report ORNL-TM-728; 1965.
3. Robertson, R. C. Technical Report ORNL-4541; 1971.
4. Status of small reactor designs without on-site refuelling; Technical Report; IAEA-TECDOC-1536; 2007.
5. Delpech, S.; Merle-Lucotte, E.; Heuer, D.; *et al. J. Fluor. Chem.* **2009**, *130*, 11–17.
6. Zherebtsov, A. L.; Ignatiev, V. V. Experimental mock-up of accelerator-based facility for transmutation of radioactive waste and conversion of military plutonium; Technical Report; Nr. 1606, Annual Report; 2006.
7. MacPherson, H. G. *Nucl. Sci. Eng.* **1985**, *90*, 374.
8. Grimes, W. R.; Cuneo, D. R. *Reactor Handbook;* Materials, Interscience: New York, 1960; Vol. I, Chapter 17, p 425.
9. Grimes, W. R. *Nucl. Appl. Technol.* **1970**, *8*, 37.
10. Haubenreich, P. N.; Engel, J. R. *Nucl. Appl. Technol.* **1970**, *8*, 118–133.
11. Mourogov, A.; Bokov, P. M. *Energ. Convers. Manag.* **2006**, *47*, 2761.
12. Gruppelaar, H.; Kloosterman, J. L.; Konings, R. J. M. Advanced Technologies for the Reduction of Nuclear Waste, Netherlands Energy Research Foundation ECN; 1998.
13. Mathieu, L. Ph. D. Thesis, France (in French), 2005.
14. Mathieu, L.; *et al.* Proposition for a very simple thorium molten salt reactor. In *Global Conference*, Tsukuba, Japan, 2005.

15. Mathieu, L.; *et al. Progr. Nucl. Energ.* **2006**, *48*, 664–679.
16. Merle-Lucotte, E.; *et al.* Fast thorium molten salt reactors started with plutonium. In *Proceedings of the International Congress on Advances in Nuclear Power Plants (ICAPP)*, Reno, NV, 2006.
17. Merle-Lucotte, E.; Heuer, D.; Brun, C. L.; Allibert, M.; Ghetta, V. The TMSR as Actinide Burner and Thorium Breeder, Note LPSC 07-37; 2007.
18. Salanne, M.; Simon, C.; Turq, P. *J. Phys. Chem. B* **2007**, *111*, 4678–4684.
19. Toth, L. M.; Gilpatrick, L. O. Technical Report ORNL-TM-4056; 1972.
20. Dracopolous, V.; Gilbert, B.; Børrensen, B.; Photiadis, G. M.; Papatheodorou, G. N. *J. Chem. Soc. Faraday Trans.* **1997**, *93*, 3081.
21. Dracopolous, V.; Gilbert, B.; Papatheodorou, G. N. *J. Chem. Soc. Faraday Trans.* **1998**, *94*, 2601.
22. Barton, C. J. *J. Phys. Chem.* **1960**, *64*, 306.
23. Rosenthal, M. W.; Briggs, R. B.; Kasten, P. R. Technical Report ORNL-4449; 1970.
24. van der Meer, J.; Konings, R. J. M.; Jacobs, M. H. G.; Oonk, H. A. J. *J. Nucl. Mater.* **2005**, *344*, 94–99.
25. Beneš, O.; Konings, R. J. M. *J. Chem. Thermodyn.* **2009**, *41*, 1086–1095.
26. Roy, D. M.; Roy, R.; Osborn, E. F.; Am, J. *Ceram. Soc.* **1954**, *37*, 300.
27. Thoma, R. E.; Insley, H.; Friedman, H. A.; Hebert, G. M. *J. Nucl. Mater.* **1968**, *27*, 166.
28. Romberger, K. A.; Braunstein, J.; Thoma, R. E. *J. Phys. Chem.* **1972**, *76*, 1154.
29. Holm, J. L.; Kleppa, O. J. *Inorg. Chem.* **1969**, *8*, 207.
30. van der Meer, J. P. M.; Konings, R. J. M.; Hack, K.; Oonk, H. A. J. *Chem. Mater.* **2006**, *18*, 510–517.
31. Beneš, O.; Konings, R. J. M. *J. Nucl. Mater.* **2008**, *377*(3), 449–457.
32. Barton, C. J.; Strehlow, R. A. *J. Inorg. Nucl. Chem.* **1961**, *18*, 143–149.
33. Barton, C. J.; Redman, J. D.; Strehlow, R. A. *J. Inorg. Nucl. Chem.* **1961**, *20*, 45–49.
34. Thoma, R. E.; Insley, H.; Friedman, H. A.; Weaver, C. F. *J. Phys. Chem.* **1960**, *64*, 865.
35. Thoma, R. E.; Insley, H.; Landau, B. S.; Friedman, H. A.; Grimes, W. R. *J. Phys. Chem.* **1959**, *63*, 1266.
36. van der Meer, J.; Konings, R. J. M.; Oonk, H. A. J. *J. Nucl. Mater.* **2006**, *357*, 48–57.
37. Barton, C. J. *J. Phys. Chem.* **1960**, *64*, 306–309.
38. Mailen, J. C.; Smith, F. J.; Ferris, L. M. *J. Chem. Eng. Data* **1971**, *16*, 68–74.
39. International Scientific Technical Centre, Moscow; Technical Report; ISTC Project #1606 Final Report; July 2004.
40. Ignatiev, V.; Merzlyakov, A.; Subbotin, V.; Panov, A.; Golovatov, Y. *Atomnaya energiya* **2006**, *101*, 364–372.
41. Ignatiev, V.; Feynberg, O.; Smirnov, V.; Tataurov, A.; Vanukova, G.; Zakirov, R. In *Proceedings of ICENES-2005*, Brussels, Belgium, Aug 21–26, 2005.
42. Thoma, R. E. *Advances in Molten Salt Chemistry;* Plenum: New York, NY, 1975; Vol. 3, Chapter 6, p 275.
43. Selivanov, V. G.; Stender, V. V. *Russ. J. Inorg. Chem.* **1958**, *2*, 279–282.
44. Barton, C. J.; Gilpatrick, L. O.; Bommann, J. A.; Stone, H. H.; McVay, T. N.; Insley, H. *J. Inorg. Nucl. Chem.* **1970**, *33*, 337–344.
45. Bergmann, A. G.; Dergunov, E. P. *Dokl. Ac. Sc. URSS* **1941**, *31*, 753.
46. Sangster, J.; Pelton, A. D. *J. Phase Equil.* **1991**, *12*, 511.
47. Chartrand, P.; Pelton, A. D. *Metall. Trans.* **2001**, *32A*, 1385.
48. Beneš, O.; Konings, R. J. M. *Comput. Coupl. Phase Diagrams Thermochem.* **2008**, *32*, 121–128.
49. Beneš, O.; Beilmann, M.; Konings, R. J. M. *J. Nucl. Mater.* **2010**, *405*, 186–198.
50. Sood, D. D.; Iyer, P. N.; Prasad, R.; *et al. Nucl. Technol.* **1975**, *27*, 411–416.
51. Blanke, B. C.; Bousquet, E. N.; Curtis, M. L.; Murphy, E. L. Technical Report USAEC MLM-1086; 1956.
52. Cantor, S.; Ward, W. T.; Moynihan, C. T. *J. Chem. Phys.* **1969**, *50*, 2874.
53. Cantor, S. Technical Report ORNL-TM-4308; 1971.
54. Cohen, S. I.; Jones, T. N. Technical Report ORNL-2278; 1957.
55. Abe, Y.; Kosugiyama, O.; Nagashima, A. *J. Nucl. Mater.* **1981**, *99*, 173–183.
56. Desyatnik, V. N.; Nechayev, A. I.; Chervinskii, Y. F. *Zh. Prikl. Khim.* **1981**, *54*, 2310–2312.
57. Porter, B.; Meaker, R. E. Technical Report BMI RI-6836; 1966.
58. Hill, D. G.; Cantor, S.; Ward, W. T. *J. Inorg. Nucl. Chem.* **1967**, *29*, 241–243.
59. Chervinskii, Y. F.; Desyatnik, V. N.; Nechaev, A. I. *Zh. Fiz. Khim.* **1982**, *56*, 1946–1949.
60. Desyatnik, V. N.; Nechaev, A. I.; Chervinskii, Y. F. *Russ. J. Phys. Chem.* **1979**, *53*, 986–988.
61. van der Meer, J.; Konings, R. J. M. *J. Nucl. Mater.* **2007**, *360*, 16–24.
62. Mackenzie, J. D. *J. Phys. Chem.* **1960**, *64*, 306–309.
63. Briant, R. C.; Weinberg, A. M. *Nucl. Sci. Eng.* **1957**, *2*, 797–803.
64. Powers, W. D.; Cohen, S. I.; Greene, N. D. *Nucl. Sci. Eng.* **1963**, *71*, 200–211.
65. Khokhlov, V.; Ignatiev, V.; Afonichkin, V. *J. Fluor. Chem.* **2009**, *130*, 30–37.
66. Janz, G. J. *J. Phys. Chem. Ref. Data* **1988**, *17*(Suppl. 2), 21–309.
67. Kirshenbaum, A. D.; Cahill, J. A. *J. Chem. Eng. Data* **1962**, *7*, 98–99.
68. Smirnov, M. V.; Khokhlov, V. A.; Antonov, A. A. *Viscosity of Molten Alkali Halides and Their Binary Mixtures*; Nauka: Moscow, 1979; p 102.
69. Ignatiev, V.; Merzliakov, A.; Afonichkin, V.; *et al.* In *Proceedings of the 7th Exchange Meeting on Actinide and Fission Product Partitioning Trans-Mutation*, Jeju, Korea, Sept 9–14, 2002; pp 581–590.
70. Ignatiev, V.; Grebenkine, K.; Subbotin, V.; *et al.* In *Proceedings of the International Symposium on Ionic Liquids*, Carry le Rouet, France, Jun 26–28, 2003; pp 203–310.
71. Chrenková, M.; Daněk, V.; Vasiljev, R.; Silný, A.; Kremetsky, V.; Polyakov, E. *J. Mol. Liq.* **2003**, *102*, 213–226.
72. Cantor, S.; Cooke, J. W.; Dworkin, A. S.; Robbins, G. D.; Thoma, R. E.; Watson, G. M. Technical Report ORNL-TM-2316; Aug 1968.
73. Douglas, T. B.; Payne, W. H. *J. Res. NBS* **1969**, *73A*, 479.
74. Cooke, J. W.; Hoffman, H. W.; Keyes, J. J. Technical Report ORNL-TM-4396; 1969.
75. Kato, Y.; Furukawa, K.; Araki, N.; Kato, Y. *High Temp. High Pres.* **1983**, *15*, 191–198.
76. Araki, N.; Kato, Y. *Research on Thorium Fuel, Ministry of Education*; Science and Culture: Tokyo, Japan, 1987; pp 83–86.
77. Smirnov, M. V.; Khokhlov, V. A.; Filatov, E. F. *Electrochim. Acta* **1987**, *32*, 1019–1026.
78. Cantor, S.; Roberts, C. E.; McDuffie, H. F. Technical Report ORNL-4229; Dec 1967.
79. Beneš, O.; Konings, R. J. M. *J. Fluor. Chem.* **2009**, *130*, 22–29.

80. Rosenthal, M. W.; Haubenreich, P. N.; Briggs, R. B. Technical Report ORNL-4812; 1972.
81. Bamberger, C. E.; Baes, C. F., Jr. *J. Nucl. Mater.* **1970**, *35*, 117.
82. Bamberger, C. E.; Ross, R. G.; Baes, C. F., Jr. *J. Inorg. Nucl. Chem.* **1971**, *33*, 767.
83. Baes, C. F., Jr. *Nucl. Metall.* **1969**, *15*, 617.
84. Rosenthal, M. W.; Briggs, R. B.; Haubenreich, P. N. Technical Report ORNL-4782; 1972.
85. Rosenthal, M. W.; Briggs, R. B.; Haubenreich, P. N. Technical Report ORNL-4728; 1971.
86. Rosenthal, M. W.; Briggs, R. B.; Haubenreich, P. N. Technical Report ORNL-4676; 1971.
87. Rosenthal, M. W.; Briggs, R. B.; Haubenreich, P. N. Technical Report ORNL-4622; 1971.
88. Rosenthal, M. W.; Briggs, R. B.; Kasten, P. R. Technical Report ORNL-4548; 1970.
89. Baes, C. F., Jr. In *Proceedings of the Symposium on Thermodynamics*, Vienna, 1966; pp 409–433.
90. Baes, C. F., Jr. In *Symposium on Reprocessing of Nuclear Fuels*, Iowa State University, Ames, IA, 1969; CONF-690801, pp 617–654.
91. Baes, C. F., Jr. *J. Nucl. Mater.* **1974**, *51*, 149–162.
92. Hitch, B. F.; Baes, C. F., Jr. *Inorg. Chem.* **1969**, *8*, 201.
93. Chamelot, P.; Massot, L.; Hamel, C.; Nourry, C.; Taxil, P. *J. Nucl. Mater.* **2007**, *360*, 64–74.
94. Hammel, C.; Chamelot, P.; Laplace, A.; Walle, E.; Dugne, O.; Taxil, P. *Electrochim. Acta* **2007**, *52*, 3995–4003.
95. Blankenship, F. F. Technical Report ORNL-3708; 1964.
96. Grimes, W. R.; Smith, N. V.; Watson, G. M. *J. Phys. Chem.* **1958**, *62*, 862–866.
97. Blander, M.; Grimes, W. R.; Smith, N. V.; Watson, G. M. *J. Phys. Chem.* **1959**, *63*, 1164–1167.
98. Watson, G. M.; Evans, R. B.; Grimes, W. R.; Smith, N. V. *J. Chem. Eng. Data* **1962**, *7*, 285–287.
99. Engel, J. R.; Bauman, H. F.; Dearing, J. F.; Grimes, W. R.; McCoy, J. H. E. Technical Report ORNL-TM-6415; 1979.
100. Compere, E. L.; Kirslis, S. S.; Bohlmann, E. G.; Blankenship, F. F.; Grimes, W. R. Technical Report ORNL-4865; 1975.
101. Engel, J. R.; Bauman, H. F.; Dearing, J. F.; Grimes, W. R.; McCoy, H. E.; Rhoades, W. A. Technical Report ORNL-TM-7207; 1980.
102. Briggs, R. B. Technical Report ORNL-3708; 1964.
103. Koger, J. W. Technical Report ORNL-TM-4286; 1972.
104. Rosenthal, M. W.; Briggs, R. B.; Kasten, P. R. Technical Report ORNL-4254; 1968.
105. Keiser, J. R. Technical Report ORNL-TM-6002; 1977.